

Structure formation from non-Gaussian initial conditions: multivariate biasing, statistics, and comparison with N-body simulations

Tommaso Giannantonio* and Cristiano Porciani

Argelander-Institut für Astronomie der Universität Bonn, Auf dem Hügel 71, D-53121 Bonn, Germany

We study structure formation in the presence of primordial non-Gaussianity of the local type with parameters f_{NL} and g_{NL} . We show that the distribution of dark-matter halos is naturally described by a multivariate bias scheme where the halo overdensity depends not only on the underlying matter density fluctuation δ but also on the Gaussian part of the primordial gravitational potential φ . This corresponds to a non-local bias scheme in terms of δ only. We derive the coefficients of the bias expansion as a function of the halo mass by applying the peak-background split to common parameterizations for the halo mass function in the non-Gaussian scenario. We then compute the halo power spectrum and halo-matter cross spectrum in the framework of Eulerian perturbation theory up to third order. Comparing our results against N-body simulations, we find that our model accurately describes the numerical data for wavenumbers $k \leq 0.1 - 0.3 h \text{ Mpc}^{-1}$ depending on redshift and halo mass. In our multivariate approach, perturbations in the halo counts trace φ on large scales and this explains why the halo and matter power spectra show different asymptotic trends for $k \rightarrow 0$. This strongly scale-dependent bias originates from terms at leading order in our expansion. This is different from what happens using the standard univariate local bias where the scale-dependent terms come from badly behaved higher-order corrections. On the other hand, our biasing scheme reduces to the usual local bias on smaller scales where $|\varphi|$ is typically much smaller than the density perturbations. We finally discuss the halo bispectrum in the context of multivariate biasing and show that, due to its strong scale and shape dependence, it is a powerful tool for the detection of primordial non-Gaussianity from future galaxy surveys.

PACS numbers: 98.65.Dx, 98.80.Cq

I. INTRODUCTION

Measurements of the cosmic microwave background (CMB) anisotropies have confirmed the hypothesis that the present inhomogeneities in the matter density were seeded by small fluctuations at primordial times [1]. Such perturbations, which are expected to be created as quantum vacuum fluctuations, have been generally modeled with the simple statistical assumption of being a Gaussian random field with nearly scale invariant power spectrum [2].

The inflationary mechanism is often invoked to describe the early universe, but the details remain debated [3]. In the simplest single-field, slow-roll model, small curvature (adiabatic) perturbations are generated with a nearly Gaussian distribution [4, 5]. However in other models such as the curvaton scenario [6–8] some additional fields would decay at later times, producing larger non-Gaussianity [9–11]; cyclic or ekpyrotic universes without inflation could also produce large non-Gaussianities during their contracting phase [12, 13]. Furthermore, multi-field models can in general produce isocurvature modes of the perturbations [14]. See [15] for a review and [16] for recent updates and future prospects.

The first observable predictions from inflation — flatness and the near scale invariance of the power spectrum of the perturbations — have been under scrutiny for some time from observations of both the large scale structure (LSS) [17] and the CMB [1]. Fairly strict constraints on the adiabaticity of the primordial perturbations also exist [18], while their Gaussian distribution has only recently become testable.

Although other possibilities exist (see [19] for a review), many models produce primordial non-Gaussianity of the *local type* where the Bardeen’s potential Φ can be expressed in terms of an auxiliary Gaussian potential φ as

$$\Phi(\mathbf{x}) = \varphi(\mathbf{x}) + \sum_{j=2}^{\infty} Q_{\text{NL}j} [\varphi^j(\mathbf{x}) - \langle \varphi^j(\mathbf{x}) \rangle], \quad (1)$$

where the series will be in practice truncated at some finite order N , and the odd momenta of the Gaussian potential φ vanish by definition. The first parameter $Q_{\text{NL}2}$, usually dubbed f_{NL} , quantifies the leading-order departure from

*Electronic address: giannant@AstroDO.Tuni-bonn.DOTde, porciani@AstroDO.Tuni-bonn.DOTde

purely Gaussian initial conditions through the irreducible three-point function or the bispectrum of the potential. While standard inflation forecasts a slow-roll suppressed, primordial $|f_{\text{NL}}| \ll 1$, subsequent evolutionary processes are expected to increase the amount of non-Gaussianity up to $|f_{\text{NL}}| \sim 1$ [20]. On the other hand, more complex models can produce $|f_{\text{NL}}| \gg 1$, although the actual predicted values vary. The second parameter $Q_{\text{NL}3}$, generally called g_{NL} , quantifies the next higher order contribution and is related to the irreducible four-point function or the trispectrum of the potential. Since $\varphi \sim 10^{-5}$, this contribution can be important only if g_{NL} is big, $g_{\text{NL}} \gtrsim f_{\text{NL}}^2$. This is plausible in the interactive curvaton model [21–23] and in other multi-field scenarios [24, 25].

The traditional method to constrain primordial non-Gaussianity has been the three-point statistics of CMB anisotropies. The current limits from WMAP are $-9 < f_{\text{NL}} < 111$ at the 95% c.l. [1]. Different analyses of the same data found $-178 < f_{\text{NL}} < 64$ using Minkowski functionals [1], $-4 < f_{\text{NL}} < 80$ using an optimized estimator [26], and $-18 < f_{\text{NL}} < 80$ from wavelet decomposition [27], while a detection ($27 < f_{\text{NL}} < 247$) was claimed by [28]. Constraints on g_{NL} are $-5.6 \cdot 10^5 < g_{\text{NL}} < 6.4 \cdot 10^5$ [29]. The Planck satellite is expected to reduce the uncertainty to $\sigma(f_{\text{NL}}) \sim 5$ [30]. This result will be nearly cosmic-variance limited, and further significant improvements from CMB studies will be difficult to achieve. This reason, together with the desire of having independent results, affected by different systematics, provided the motivation to study the detectability of primordial non-Gaussianity from the LSS. In this case, however, the non-linear growth of density perturbations can superimpose a new non-Gaussian signal onto the primordial one [31], which may be difficult to retrieve. Determining the mass distribution of galaxy clusters at low and high redshift provides a way to circumvent this problem [32, 33]. However, due to the low-number statistics, these methods have been so far less successful than the CMB. Upcoming surveys such as PanSTARRS, DES, LSST, ADEPT, EUCLID, JDEM or eROSITA, WFXT and SPT are expected to substantially improve the situation.

A new technique, based on linear perturbation theory, has been recently introduced by [34] (Dal07 in the following). These authors showed that local non-Gaussianity breaks the independence of small and large scales density fluctuations. As a consequence, the clustering of dark matter halos is altered, becoming enhanced on large scales for a positive f_{NL} . An analytical derivation of the corresponding scale-dependent bias has been also presented by [35–38], together with some observational constraints on f_{NL} from existing data of the clustering of galaxies and their correlation with the CMB anisotropies. Using luminous red galaxies and quasars from the SDSS, Slosar et al. [36] obtained $-29 < f_{\text{NL}} < 69$, competitive with the CMB results. The first constraints on g_{NL} from the LSS give $-3.5 \cdot 10^5 < g_{\text{NL}} < 8.2 \cdot 10^5$ [39], *assuming* $f_{\text{NL}} = 0$.

N-body simulations show only approximate agreement with the model by Dal07 [40–42]. In particular, the power spectrum of dark-matter halos seems to scale with the wavenumber and the f_{NL} parameter in a different way than predicted. This discrepancy provides the main motivation for this paper where we study the effect of non-Gaussian initial conditions on the clustering of halos in the weakly non-linear regime of perturbation growth. Applying the peak-background split technique, we show that the halo distribution on large scales is naturally described by a *bivariate local biasing scheme*, where the halo overdensity is expanded in a Taylor series of both the matter perturbations δ and the primordial Gaussian potential φ . Since φ and δ are related by the Poisson equation, this can be equivalently seen as a non-local description in terms of δ only. This reduces to the usual univariate *local* bias (where halo overdensities are expanded in series of δ only) for Gaussian initial conditions and, in general, on small scales. Using standard (Eulerian) perturbation theory (SPT) up to third order to account for the non-linear growth of density fluctuations, we show that our new biasing scheme leads to the presence of several new terms in the halo power spectrum and bispectrum. We show that our results reduce to the usual Gaussian solution in the limit $f_{\text{NL}} \rightarrow 0$, and to the results by Dal07 (revised as in [36, 40]) if we only consider the leading-order terms. Finally, we compare our theory with the N-body simulations by [41] (hereafter PPH08) and find that our model can explain the numerical results to a much greater accuracy than both linear and univariate local theories.

Our paper differs from the recent work by [43–46] which is based on the assumption that fluctuations in the halo number counts only depend on the local mass density. By ignoring the expansion in the potential φ and only considering the dependence on the matter density perturbations δ , one would obtain different results which do not reduce to the model by Dal07 to leading order and do not match the simulations as well; in this case higher-order terms in the halo power spectrum grow bigger than the first-order contribution on large scales, thus casting doubts on the validity of the perturbative expansion. Our approach is also different from the work by [47] because we use SPT without applying any renormalization technique. Renormalizing the bias removes any undesired dependence on the cutoff scale introduced to regularize loop corrections in SPT; however, in such a model the bias coefficients cannot be predicted and should be used as fitting parameters to match observations or simulations.

The plan of this paper is as follows. In Section II we summarize the main biasing schemes which have been proposed to describe the distribution of different tracers of the LSS. In Section III we introduce some models for the halo mass function arising from non-Gaussian initial conditions and compare them against the N-body results by PPH08. We then describe in Section IV how a multivariate bias scheme naturally emerges by applying the peak-background split technique to compute halo overdensities in the non-Gaussian case. In Section V we give a short summary of the statistical properties of non-Gaussian density fields. After computing the halo power spectrum and the halo-matter

cross spectrum in our multivariate biasing scheme in Section VI, we test our theoretical models against the N-body simulations by PPH08. We derive the halo bispectrum in Section VII, and conclude in Section VIII.

II. TRACERS OF THE LARGE-SCALE STRUCTURE AND BIASING

The large-scale structure of the Universe can be described in terms of different tracers: mass, luminosity, galaxy counts. In this paper we will consider dark-matter halos and mass but our formalism can be straightforwardly extended to any other tracer. Let us consider the mass overdensity field $\delta(\mathbf{x})$ and the corresponding density contrast of dark-matter halos in a given mass range $\delta_h(\mathbf{x})$. After smoothing both fields on a relatively large scale R , it is reasonable to expect that δ_h is a local function of δ that can be expanded in a Taylor series as follows:

$$\delta_h(\mathbf{x}) = b_0 + b_1\delta(\mathbf{x}) + b_2\delta^2(\mathbf{x})/2! + b_3\delta^3(\mathbf{x})/3! + \dots, \quad (2)$$

where the bias coefficients b_i are in principle scale and mass dependent [48]. This approximation neglects stochasticity in the δ_h vs. δ relation and is thus dubbed local deterministic biasing. Numerical simulations from Gaussian initial conditions show that it is accurate on scales of the order of 10 Mpc and larger [49]. In the following sections we will show that Eq. (2) does not hold in the presence of primordial non-Gaussianity of the local type and we will explain how it should be modified.

Note that, in general, the bias coefficients in Eq. (2) are not independent as the mean halo overdensity must vanish and δ_h must assume the value -1 when $\delta = -1$. In order to build a predictive theory, the values for the bias coefficients should be derived from a model. A common approach is to use the peak-background split technique [2, 50–52] where the mass perturbations are divided into fine-grained (peak) and coarse-grained (background) components. The key idea is to ascribe halo formation to the collapse of the high-frequency modes, while the large-scale distribution and motion of these condensations is determined by the low-frequency modes. Starting from a model for the conditional halo mass function (i.e. the mass function in regions where the background density assumes a specific value), the peak-background split gives an expression for the halo distribution in Lagrangian space (i.e. in the linear density field, δ_1):

$$\delta_h^L(\mathbf{q}) = b_0^L + b_1^L\delta_1(\mathbf{q}) + b_2^L\delta_1^2(\mathbf{q})/2! + b_3^L\delta_1^3(\mathbf{q})/3! + \dots, \quad (3)$$

where the bias coefficients b_i^L are obtained from the i -th order derivatives of the conditional mass function with respect to the background density contrast (see Section IV for further details). When the background scale is much larger than the Lagrangian size of the halos, the Lagrangian bias parameters show very little dependence on the background scale and the unconditional mass function can be safely used to derive them [53]. We will follow this approach in this paper.

In the absence of large-scale velocity bias, the halo density in the evolved Eulerian space is given by

$$1 + \delta_h(\mathbf{x}) = [1 + \delta_h^L(\mathbf{q})][1 + \delta(\mathbf{x})] \quad (4)$$

where \mathbf{q} is the Lagrangian position of the fluid elements that moved to the Eulerian location \mathbf{x} [52]. Note that the conversion between Lagrangian and Eulerian quantities is non-local, non-linear and stochastic as it depends on the displacement $\mathbf{x} - \mathbf{q}$ and on both the initial and the evolved fields δ_1 and δ . Therefore, the local Lagrangian biasing scheme given in Eq. (3) will not generally be compatible with Eq. (2). Catelan et al. [54] showed that these two bias models give rise to different shapes of the halo bispectrum that could then be used to distinguish between them using data from observations or simulations. A simplified approach is obtained by assuming that the long-wavelength modes of the density field evolve locally according to the spherical collapse model [51, 55]. In this case, Eqs. (3) and (2) are fully compatible and the Eulerian bias parameters can be written in terms of the Lagrangian ones (see Eq. (38) in Section IV). In particular, $b_1 = 1 + b_1^L$. This equation is completely general as it derives from mass conservation [51, 52]. However, the relation between higher-order Eulerian and Lagrangian bias parameters depends on the adopted dynamics for the background density field. A perturbative calculation of the power spectrum for local Lagrangian biasing in the Gaussian scenario has been presented by [56]. The equivalent result for the local Eulerian bias scheme has been derived by [57]. In this paper we generalize this latter result to non-Gaussian initial conditions of the local type and also present a model for the bias coefficients as a function of the halo mass. The derivation of a multivariate bias scheme and the corresponding calculations of the halo power spectrum and bispectrum constitute our main results.

III. HALO MASS FUNCTION AND PRIMORDIAL NON-GAUSSIANITY

The number density \mathcal{N} of halos of mass M at a redshift z is described by the mass function

$$n = \frac{d\mathcal{N}}{dM} = f\left(\frac{\delta_c}{\sigma}\right) \frac{\bar{\rho}}{M^2} \left| \frac{d \ln \sigma^{-1}}{d \ln(M)} \right|, \quad (5)$$

where $\delta_c \simeq 1.686$ is the threshold for the linear density contrast which corresponds to the collapse of spherical perturbations. In Eq. (5), σ^2 denotes the variance of the linear density field, calculated as

$$\sigma^2(M, z) = \frac{D^2(z)}{2\pi^2} \int k^2 P_0(k) W_f^2(k, M) dk, \quad (6)$$

with $P_0(k)$ the linear matter power spectrum at $z = 0$, $D(z)$ the linear growth factor of density fluctuations normalized to unity today, and $W_f(k, M)$ a filter function with mass resolution M . We use a top-hat filter in real space with radius $R_f = [3M/(4\pi\bar{\rho})]^{1/3}$, where $\bar{\rho}$ is the average density of the Universe. The analytical form of the distribution $f(\delta_c/\sigma)$ can be derived from a theoretical model or by fitting numerical data. We list below some possible choices for this function.

A. Gaussian mass functions

Press-Schechter (PS) For reference we first consider the Press-Schechter theory [58], in which the mass function deriving from Gaussian initial conditions is given by

$$f_{\text{PS}}\left(\frac{\delta_c}{\sigma}\right) = \sqrt{\frac{2}{\pi}} \frac{\delta_c}{\sigma} e^{-\frac{\delta_c^2}{2\sigma^2}}. \quad (7)$$

It is well known that this model gives only a rough approximation to numerical data (see Fig. 1). The Press-Schechter theory can be improved by introducing extra parameters in the mass function and fitting them against numerical simulations. This approach has been followed e.g. by Jenkins et al. [59], Warren et al. (W) [60], Tinker et al. [61].

Sheth-Tormen (ST) The Press-Schechter theory is based on the spherical collapse model. This can be improved upon by considering the collapse of ellipsoidal perturbations and fitting some new parameters against numerical simulations. [53, 62]. The final result, known as the ST mass function, is

$$f_{\text{ST}}\left(\frac{\delta_c}{\sigma}\right) = A \sqrt{\frac{2\alpha}{\pi}} \left[1 + \left(\alpha \frac{\delta_c^2}{\sigma^2} \right)^{-p} \right] \frac{\delta_c}{\sigma} e^{-\frac{\alpha\delta_c^2}{2\sigma^2}}, \quad (8)$$

where the extra parameters are $\alpha = 0.707$, $p = 0.3$ and A is obtained by requiring that all the mass is collapsed into halos, which gives $A = 0.322$.

B. Non-Gaussian mass functions

In the simplest case, local non-Gaussianity is described by truncating Eq. (1) after the second order term, which corresponds to:

$$\Phi(\mathbf{q}) = \varphi(\mathbf{q}) + f_{\text{NL}} [\varphi^2(\mathbf{q}) - \langle \varphi^2(\mathbf{q}) \rangle]. \quad (9)$$

It can be shown that the halo mass function is very sensitive to the value of f_{NL} . For positive (negative) values of f_{NL} , its high-mass tail becomes more (less) prominent than in the Gaussian case. To first-order in the non-linearity parameter f_{NL} , it is possible to account for this effect by considering the skewness of the density perturbations, defined as $S_3(\sigma) = \langle \delta^3 \rangle / \sigma^4$.

Matarrese-Verde-Jiménez (MVJ) The Press-Schechter theory can be generalized to non-Gaussian initial conditions by using the saddle point approximation to calculate the probability for the linear density field to be above δ_c [32]. In this case, one obtains:

$$f_{\text{MVJ}}\left(\frac{\delta_c}{\sigma}\right) = \sqrt{\frac{2}{\pi}} e^{-\delta_c^2/(2\sigma^2)} \left| \frac{\delta_c^3}{6\sigma\delta_*} \frac{dS_3(\sigma)}{d \ln \sigma} + \frac{\delta_*}{\sigma} \right|, \quad (10)$$

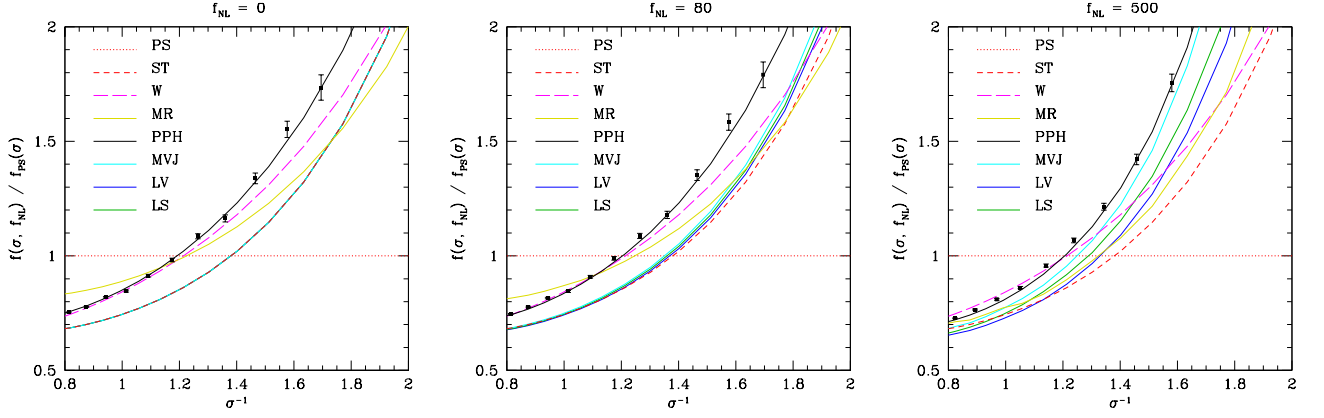


FIG. 1: Comparison of different models for the halo mass function originating from Gaussian (dashed) and non-Gaussian (solid) initial conditions with the N-body data by PPH08. From left to right, the different panels refers to $f_{\text{NL}} = 0, 80, 500$. Note that all non-Gaussian models (with the exception of MR) have been rescaled by the ratio $f_{\text{ST}}/f_{\text{PS}}$, and thus coincide with the ST function in the leftmost panel.

where the new parameter δ_* is defined as $\delta_* \equiv \delta_c \sqrt{1 - \delta_c S_3(\sigma)/3}$. Since the ST model outperforms the PS one in the Gaussian case, it is standard practice to define a new mass function as $f_{\text{MVJ}} \rightarrow f_{\text{MVJ}} \cdot f_{\text{ST}}/f_{\text{PS}}$. A further modification which has been suggested by [42] to improve the agreement with numerical simulations is to correct the collapse threshold δ_c by a factor $\sqrt{a} = \sqrt{0.8}$ in the expression $f_{\text{MVJ}}/f_{\text{PS}}$. In what follows we will adopt both corrections. A similar result was derived by [38] using a different approach.

LoVerde et al. (LV) Another way to generalize the PS model is to use the Edgeworth expansion to approximate the probability distribution function for the linear density contrast [33]. This gives:

$$f_{\text{LV}}\left(\frac{\delta_c}{\sigma}\right) = \sqrt{\frac{2}{\pi}} e^{-\delta_c^2/(2\sigma^2)} \left\{ \left[\frac{\delta_c}{\sigma} + S_3(\sigma) \frac{\sigma}{6} \left(\frac{\delta_c^4}{\sigma^4} - 2 \frac{\delta_c^2}{\sigma^2} - 1 \right) \right] + \frac{1}{6} \frac{dS_3(\sigma)}{d \ln \sigma} \sigma \left(\frac{\delta_c^2}{\sigma^2} - 1 \right) \right\}. \quad (11)$$

As for the MVJ case, we will use an effective form of this mass function expressing the correction to the ST formula: $f_{\text{LV}} \rightarrow f_{\text{LV}} \cdot f_{\text{ST}}/f_{\text{PS}}$, with the further modification of correcting the collapse threshold δ_c by a factor $\sqrt{a} = \sqrt{0.8}$ in the ratio $f_{\text{LV}}/f_{\text{PS}}$.

Maggiore-Riotto (MR) Maggiore & Riotto [63] computed the halo mass function by solving the excursion set problem for non-Markovian processes with a path-integral approach, and found

$$f_{\text{MR}}\left(\frac{\delta_c}{\sigma}\right) = (1 - \tilde{\kappa}) \sqrt{\frac{2}{\pi}} \frac{\sqrt{a} \delta_c}{\sigma} e^{-a \delta_c^2/(2\sigma^2)} \left[1 + \frac{\sigma^2}{6 \sqrt{a} \delta_c} h_{\text{NG}}(\sigma) \right] + \frac{\tilde{\kappa}}{\sqrt{2\pi}} \frac{\sqrt{a} \delta_c}{\sigma} \Gamma\left(0, \frac{a \delta_c^2}{2\sigma^2}\right). \quad (12)$$

Here $\Gamma(0, x)$ is the incomplete Gamma function, the additional parameters are $a \simeq 0.8$ and $\tilde{\kappa} = a\kappa$ where $\kappa \simeq 0.4562 - 0.0040 R_f$ with R_f the smoothing scale. Primordial non-Gaussianity affects the function

$$h_{\text{NG}}(\sigma) = \frac{a^2 \delta_c^4}{\sigma^4} S_3(\sigma) - \frac{a \delta_c^2}{\sigma^2} \left[2S_3(\sigma) + U_3(\sigma) - \frac{dS_3}{d \ln \sigma} \right] - \left[S_3(\sigma) + U_3(\sigma) + V_3(\sigma) + \frac{dS_3}{d \ln \sigma} + \frac{dU_3}{d \ln \sigma} \right], \quad (13)$$

where U_3 and V_3 are given by:

$$U_3(\sigma) = \frac{3}{\sigma^2} \left[\frac{d}{d(\sigma_1^2)} \langle \delta(\sigma_1^2) \delta^2(\sigma^2) \rangle \right]_{\sigma_1^2 = \sigma^2} \quad (14)$$

$$V_3(\sigma) = \frac{9}{2} \left[\frac{d^2}{d(\sigma_1^2)^2} \langle \delta(\sigma_1^2) \delta^2(\sigma^2) \rangle \right]_{\sigma_1^2 = \sigma^2} + 12 \left[\frac{d}{d(\sigma_1^2)} \frac{d}{d(\sigma_2^2)} \langle \delta(\sigma_1^2) \delta(\sigma_2^2) \delta^2(\sigma^2) \rangle \right]_{\sigma_1^2 = \sigma_2^2 = \sigma^2}. \quad (15)$$

The MR function does not need any ad-hoc rescaling.

Lam-Sheth (LS) An extension of the ST model to primordial non-Gaussianity has been recently proposed by [64]. In this case the mass function is written as:

$$f_{\text{LS}}\left(\frac{\delta_c}{\sigma}\right) = f_{\text{ST}}\left(\frac{\delta_c}{\sigma}\right) \left\{ 1 + \frac{\sigma S_3}{6} H_3 \left[\frac{b(\sigma)}{\sigma} \right] \right\}, \quad (16)$$

where $H_3(x) = x(x^2 - 3)$, and the mass-dependent collapse barrier is $b(\sigma) = \sqrt{a}\delta_c \left[1 + \beta (\sigma/\sqrt{a}\delta_c)^{2\gamma} \right]$, with $\beta = 0.4$, $\gamma = 0.6$, $a = 0.7$. Note that, in the case of a constant barrier, this mass function reduces to the LV one, if in the latter we neglect the term proportional to the derivative of S_3 , which is generally small.

C. Comparison with N-body simulations

In Fig. 1 we compare the theoretical mass functions presented above with the N-body data by PPH08. The halos in the simulations were identified using a friends-of-friends algorithm with linking length $b = 0.2\lambda$, where λ is the mean interparticle distance. Consistently with PPH08, for our calculations we assume the WMAP5 Λ CDM model, with parameters $h = 0.701$, $\sigma_8 = 0.817$, $n_s = 0.96$, $\Omega_m = 0.279$, $\Omega_b = 0.0462$, $\Omega_\Lambda = 0.721$. We find that all the theoretical mass functions match the numerical output within $\sim 10 - 20\%$ for $f_{\text{NL}} < 500$. Most of the discrepancy originates from the fact that the ST mass function underestimates the halo counts from the simulations (left panel in Fig. 1). Indeed, the models are rather accurate in predicting the ratio between the counts in a non-Gaussian model vs. a Gaussian one (see also [40–42]). We also consider a fitting formula for the mass function that was computed by PPH08 from the very same data plotted in Fig. 1. Here we rewrite it as

$$f_{\text{PPH}}\left(\frac{\delta_c}{\sigma}\right) = \left[D + B \left(\frac{\delta_c}{1.686\sigma} \right)^A \right] \exp\left(-\frac{C\delta_c^2}{1.686^2\sigma^2} \right), \quad (17)$$

where we have explicitly introduced a dependence on the threshold collapse density δ_c , and A, B, C, D are fitting parameters which depend on f_{NL} . We use the values from Table 5 in PPH08.

In the next section, we will use the mass function to compute the halo bias parameters in the non-Gaussian scenario. Given that all the models for n are of the same quality, as a reference, we will only show the results obtained with the LV mass function and the PPH fit.

IV. HALO BIAS

A. Peak-background split

We decompose the Gaussian auxiliary potential φ into the (statistically independent) contributions of long- and short-wavelength modes:

$$\varphi(\mathbf{q}) = \varphi_l(\mathbf{q}) + \varphi_s(\mathbf{q}). \quad (18)$$

Eq. (9) then gives

$$\begin{aligned} \Phi_l &= \varphi_l + f_{\text{NL}}\varphi_l^2 - \langle \varphi^2 \rangle \\ \Phi_m &= 2f_{\text{NL}}\varphi_l\varphi_s \\ \Phi_s &= \varphi_s + f_{\text{NL}}\varphi_s^2, \end{aligned} \quad (19)$$

where the dependence on the spatial position is understood. The mixed term Φ_m contributes to the short-wavelength part but derives from the coupling of φ_l and φ_s . It vanishes for Gaussian initial conditions. When passing from real to Fourier space, the products of two fields become convolutions. Strictly speaking, the terms $\varphi_l\varphi_s$ and φ_s^2 would also contribute to the long modes Φ_l , due to the mixing of modes caused by the convolution operation. We have checked however that these additional contributions are completely subdominant.

Using the Poisson equation, $\nabla^2\Phi = A\delta$ with $A = 3\Omega_m H_0^2/(2c^2)$, for the density fluctuations we can then write

$$\begin{aligned} \delta_l &= \delta_{G_l}(1 + 2f_{\text{NL}}\varphi_l) + 2A^{-1}f_{\text{NL}}\nabla\varphi_l \cdot \nabla\varphi_l \\ \delta_m &= 2f_{\text{NL}}(\delta_{G_s}\varphi_l + \delta_{G_l}\varphi_s) + 4A^{-1}f_{\text{NL}}\nabla\varphi_l \cdot \nabla\varphi_s \\ \delta_s &= \delta_{G_s}(1 + 2f_{\text{NL}}\varphi_s) + 2A^{-1}f_{\text{NL}}\nabla\varphi_s \cdot \nabla\varphi_s, \end{aligned} \quad (20)$$

where $\nabla^2\varphi = A\delta_G$. Notice that:

$$\delta_m = 2f_{\text{NL}} \left[\frac{\delta_s - 2A^{-1}f_{\text{NL}}\nabla\varphi_s \cdot \nabla\varphi_s}{1 + 2f_{\text{NL}}\varphi_s} \varphi_l + \frac{\delta_l - 2A^{-1}f_{\text{NL}}\nabla\varphi_l \cdot \nabla\varphi_l}{1 + 2f_{\text{NL}}\varphi_l} \varphi_s \right] + 4A^{-1}f_{\text{NL}}\nabla\varphi_l \cdot \nabla\varphi_s. \quad (21)$$

In the spirit of the peak-background split [2, 50–52], the short-wavelength modes of the density field collapse to form virialized condensations (dark-matter halos) while the long-wavelength ones modulate the halo counts and are responsible for large-scale motions. In the non-Gaussian case, however, the halo collapse will also be influenced by the long-wavelength modes of φ and $\nabla\varphi$ which contribute to δ_m . In a Press-Schechter approach, modulations in δ_l will modify the threshold for halo collapse as in the Gaussian case. However, *in the presence of non-Gaussian fluctuations, the large-scale modes of the pseudo-potential will also alter the statistical properties of the small-scale modes in the density field*. This provides an additional source of biasing with respect to the Gaussian case. Suppose we want to apply the Press-Schechter algorithm to δ . The probability that the small-scale fluctuation $\delta_s + \delta_m$ is above the collapse threshold $\delta_c - \delta_l$ (probability which is obtained by averaging over δ_s) would then explicitly depend on δ_l , φ_l and $\nabla\varphi_l$. This implies that the resulting large-scale halo overdensity cannot be proportional to δ_l as in the Gaussian case (to first order). Rather, in the general case, $\delta_h \simeq b_1\delta_l + f_1\varphi_l + g_1\nabla\varphi_l \cdot \nabla\varphi_l$ plus higher-order terms. The bias coefficients are given by the Taylor expansion of the conditional mass function $n(M|\delta_l, \varphi_l, \nabla\varphi_l \cdot \nabla\varphi_l)$. Unfortunately, the models for the mass function listed in the previous section have been obtained by averaging over the entire Lagrangian volume and have no memory of the cross-talk between large and small scales. We attempted the calculation of $n(M|\delta_l, \varphi_l, \nabla\varphi_l \cdot \nabla\varphi_l)$ by adopting a Press-Schechter approach and starting from the Gaussian fields $\varphi, \nabla\varphi$ and $\nabla^2\varphi$ but we could not obtain a closed form due to the complexity of the expressions.

An approximated model can be obtained assuming that halos form from the highest peaks of δ_s .^{*} We want to implement this requirement in Eq. (20). Let us consider what the labels "short" and "long" mean in practical terms. The short part of the fields will only include a narrow shell of modes centered around the wavelength corresponding to Lagrangian size of the halos. On the other hand, the long part will be formed with all the Fourier modes with larger wavelengths. In this case, φ_s will be closely tracing $\delta_{G_s} \simeq \delta$. This implies that the high density peaks will nearly coincide with the maxima of φ_s , where $\nabla\varphi_s = 0$. In this case,

$$\delta_s + \delta_m = \delta_s \left(1 + \frac{2f_{\text{NL}}\varphi_l}{1 + 2f_{\text{NL}}\varphi_s} \right) + \frac{\delta_l - 2A^{-1}f_{\text{NL}}\nabla\varphi_l \cdot \nabla\varphi_l}{1 + 2f_{\text{NL}}\varphi_l} 2f_{\text{NL}}\varphi_s.$$

The Lagrangian size of galaxy- and cluster-sized halos ranges between 1 and 10 Mpc. This implies that $\langle \delta_s^2 \varphi_l^2 \rangle^{1/2} \gg \langle \delta_l^2 \varphi_s^2 \rangle^{1/2}$ and $\langle \varphi_l^2 \rangle \simeq \langle \varphi_s^2 \rangle$, since perturbations in the pseudo-potential are nearly scale invariant. Moreover, $f_{\text{NL}}\langle \varphi_l^2 \rangle^{1/2} \ll 1$ for the values of f_{NL} of physical interest. We thus obtain

$$\delta_s + \delta_m \simeq \delta_s (1 + 2f_{\text{NL}}\varphi_l), \quad (22)$$

i.e. the amplitude of small-scale density fluctuations is enhanced in regions where φ_l is large. Therefore, the conditional mass function $n(M|\varphi_l)$ can be computed from the unconditional one $n(M)$ by simply multiplying the r.m.s. of the density fluctuations by the factor $1 + 2f_{\text{NL}}\varphi_l$.[†] At the same time, we can use the peak-background split to derive $n(M|\delta_l, \varphi_l)$ by simply replacing δ_c with $\delta_c - \delta_l$.

In each point in Lagrangian space, we can thus define a Lagrangian halo density field as

$$\delta_h^L(\mathbf{q}) = \frac{n[M, \delta_l(\mathbf{q}), \varphi_l(\mathbf{q})]}{\bar{n}} - 1, \quad (23)$$

where the average can simply be taken as $\bar{n} = n(M, 0, 0)$. Here it is possible to replace n with f since the proportionality factors cancel out, so that we can write more explicitly

$$\delta_h^L(\mathbf{q}) = \frac{f\left(\frac{\delta_c - \delta_l(\mathbf{q})}{[1 + 2f_{\text{NL}}\varphi_l(\mathbf{q})]\sigma}\right)}{f\left(\frac{\delta_c}{\sigma}\right)} - 1. \quad (24)$$

^{*} We only assume that halo formation happens around some of the density peaks. This is different from the approach by [35, 39], in which all peaks form halos, and a one-to-one correspondence between them is assumed.

[†] Slosar et al. [36] and Afshordi and Tolley [37] derived a similar expression but notice that ours is written in terms of the non-Gaussian density field.

We can then expand the perturbations in a Taylor series in terms of *both* variables δ_l and φ_l , obtaining

$$\delta_h^L(\mathbf{q}) = \sum_{j=0}^{\infty} \sum_{m=0}^{\infty} \frac{b_{jm}^L}{j!m!} \delta_l^j(\mathbf{q}) \varphi_l^m(\mathbf{q}). \quad (25)$$

Up to third order in the perturbations, this gives:

$$\begin{aligned} \delta_h^L(\mathbf{q}) &= b_0^L + b_{10}^L \delta + b_{01}^L \varphi + \\ &+ \frac{1}{2!} (b_{20}^L \delta^2 + 2 b_{11}^L \delta \varphi + b_{02}^L \varphi^2) + \\ &+ \frac{1}{3!} (b_{30}^L \delta^3 + 3 b_{21}^L \delta^2 \varphi + 3 b_{12}^L \delta \varphi^2 + b_{03}^L \varphi^3), \end{aligned} \quad (26)$$

where all the density perturbations on the r.h.s. are Lagrangian and non-Gaussian.

Eq. (24) implies that not all the coefficients b_{jm}^L are independent. In particular, all the b_{jm}^L with $m \neq 0$ can be written in terms of the b_{j0}^L . Up to third order we have:

$$\begin{aligned} b_{01}^L &= 2 f_{\text{NL}} \delta_c b_{10}^L \\ b_{11}^L &= 2 f_{\text{NL}} (-b_{10}^L + \delta_c b_{20}^L) \\ b_{02}^L &= 4 f_{\text{NL}}^2 (-2\delta_c b_{10}^L + \delta_c^2 b_{20}^L) \\ b_{21}^L &= 2 f_{\text{NL}} (-2b_{20}^L + \delta_c b_{30}^L) \\ b_{12}^L &= 4 f_{\text{NL}}^2 (2b_{10}^L - 4\delta_c b_{20}^L + \delta_c^2 b_{30}^L) \\ b_{03}^L &= 8 f_{\text{NL}}^3 (6\delta_c b_{10}^L - 6\delta_c^2 b_{20}^L + \delta_c^3 b_{30}^L). \end{aligned} \quad (27)$$

It is important to remember that the functional form of the halo mass function accounts for the effect of non-Gaussianity on the short wavelength modes δ_s, δ_m . The bias coefficients b_{j0}^L will then depend implicitly on f_{NL} through the shape of the mass function.

B. Extension to higher-order non-Gaussianity

If the model for non-Gaussianity is extended to higher order, then Eq. (9) is replaced by Eq. (1). If we consider cubic corrections, we have the following additional contributions to Eqs. (19):

$$\begin{aligned} \Delta\Phi_l &= g_{\text{NL}} \varphi_l^3 \\ \Delta\Phi_m &= 3g_{\text{NL}} (\varphi_l^2 \varphi_s + \varphi_l \varphi_s^2) \\ \Delta\Phi_s &= g_{\text{NL}} \varphi_s^3, \end{aligned} \quad (28)$$

which correspond to the following additions in Eqs. (20):

$$\begin{aligned} \Delta\delta_l &= 3g_{\text{NL}} \varphi_l^2 \delta_{Gl} + 6A^{-1} g_{\text{NL}} \varphi_l \nabla\varphi_l \cdot \nabla\varphi_l \\ \Delta\delta_m &= 3g_{\text{NL}} \delta_{Gl} \varphi_s (2\varphi_l + \varphi_s) + 6g_{\text{NL}} A^{-1} \varphi_s \nabla\varphi_l \cdot \nabla\varphi_l \\ \Delta\delta_s &= 0, \end{aligned} \quad (29)$$

where we have already imposed the peak condition. In analogy with the previous section we thus identify the leading term as:

$$\delta_s + \delta_m \simeq \delta_s (1 + 2f_{\text{NL}}\varphi_l + 3g_{\text{NL}}\varphi_l^2). \quad (30)$$

It follows that the r.m.s. of the small-scale density fluctuations will now be altered by a factor $(1 + 2f_{\text{NL}}\varphi_l + 3g_{\text{NL}}\varphi_l^2)$ with respect to the Gaussian case. Therefore, considering $g_{\text{NL}} \neq 0$ introduces additional terms in the bias coefficients in Eq. (27), given by

$$\begin{aligned} \Delta b_{02}^L &= 6 g_{\text{NL}} \delta_c b_{10}^L \\ \Delta b_{12}^L &= 6 g_{\text{NL}} (-b_{10}^L + \delta_c b_{20}^L), \end{aligned} \quad (31)$$

while all the other bias coefficients remain unchanged (apart from the modifications due to the implicit dependence of the mass function on g_{NL} , which we do not calculate here).

Eq. (30) can be finally generalized to an arbitrary order N as

$$\delta_s + \delta_m \simeq \delta_s \sum_{j=2}^N j Q_{\text{NL}j} \varphi_l^{j-1}. \quad (32)$$

This equation shows that the leading contribution of each successive order will depend on a higher power of the potential, and its effects will therefore be smaller in amplitude. Note that $h_{\text{NL}} \equiv Q_{\text{NL}4}$ is the highest-order term that can explicitly modify the b_{ij} parameters (up to third order in the bias expansion), although all the $Q_{\text{NL}j}$ will introduce implicit dependences by modifying the halo mass function.

C. Bias from a mass function

We want now to explicitly calculate the halo bias corresponding to a given mass function. As discussed above, in the non-Gaussian case the mass function will also be explicitly dependent on the potential φ , and the halo overdensities can now be derived from Eq. (25), as a bivariate series expansion in terms of δ_l and φ_l . Since the effect of the short-wavelength modes is taken into account by the functional form of the mass function, we will henceforth drop the l indices and use the symbols δ and φ to denote the long-wavelength parts of the perturbations.

PS model For reference, we derive the bias coefficients corresponding to the simple PS mass function (see also [51])

$$\begin{aligned} b_{10}^L &= -\frac{1}{\delta_c} + \frac{\delta_c}{\sigma^2}, \\ b_{20}^L &= \frac{\delta_c^2}{\sigma^4} - \frac{3}{\sigma^2} \\ b_{30}^L &= \frac{\delta_c^3}{\sigma^6} - \frac{6\delta_c}{\sigma^4} + \frac{3}{\delta_c \sigma^2} \end{aligned} \quad (33)$$

and show their mass dependence in the right panel of Fig. 2. The remaining coefficients can be obtained using Eq. (27):

$$\begin{aligned} b_{01}^L &= \left(\frac{2\delta_c^2}{\sigma^2} - 2 \right) f_{\text{NL}} \\ b_{11}^L &= \left(\frac{2}{\delta_c} + \frac{2\delta_c^3}{\sigma^4} - \frac{8\delta_c}{\sigma^2} \right) f_{\text{NL}} \\ b_{02}^L &= 2 \left(\frac{2\delta_c^4}{\sigma^4} - 10 \frac{\delta_c^2}{\sigma^2} + 4 \right) f_{\text{NL}}^2 \\ b_{21}^L &= 2 \left(\frac{\delta_c^4}{\sigma^6} - \frac{8\delta_c^2}{\sigma^4} + \frac{9}{\sigma^2} \right) f_{\text{NL}} \\ b_{12}^L &= 2 \left(\frac{2\delta_c^5}{\sigma^6} - \frac{20\delta_c^3}{\sigma^4} + \frac{34\delta_c}{\sigma^2} - \frac{4}{\delta_c} \right) f_{\text{NL}}^2 \\ b_{03}^L &= 6 \left(\frac{4\delta_c^6}{3\sigma^6} - \frac{16\delta_c^4}{\sigma^4} + \frac{36\delta_c^2}{\sigma^2} - 8 \right) f_{\text{NL}}^3. \end{aligned} \quad (34)$$

Notice that the ‘‘usual’’ bias coefficients ($b_{10}^L, b_{20}^L, b_{30}^L$) are in this case independent from f_{NL} . This does not hold in general, since an implicit dependence on f_{NL} will be introduced by any non-Gaussian mass function.

General case To derive the bias coefficients up to the third order, we can repeat the same procedure for any other mass function. We have calculated these coefficients for all the mass functions listed in Section III finding an overall agreement in the trends with mass and with the non-linearity parameter f_{NL} . The analytic form of the bias parameters is much more complex than for the PS mass function and we will not write it explicitly. As an example, in Fig. 2 we show how the bias coefficients b_{j0}^L depend on f_{NL} and halo mass for the LV mass function and the PPH fit.

D. Lagrangian and Eulerian bias

A model for the formation of the LSS provides a relationship between the density perturbations in Lagrangian and Eulerian space. This relation is generally non-local [52] but a local approximation (where $\mathbf{x} \equiv \mathbf{q}$) suffices to

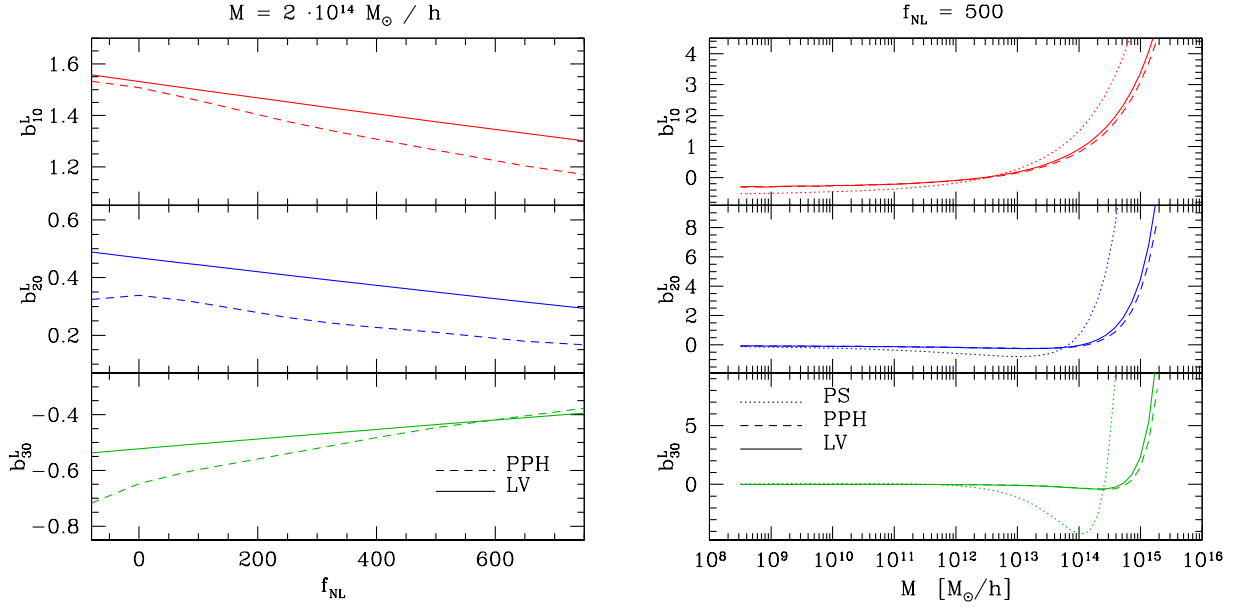


FIG. 2: Lagrangian bias factors at $z = 0$ as a function of f_{NL} for a halo mass of $2 \cdot 10^{14} M_{\odot}/h$ (left), and as a function of the halo mass, for $f_{\text{NL}} = 500$ (right). The results obtained from the PPH and LV mass functions are shown in both cases. For reference, in the right panel we also show the results obtained from the PS mass function, which does not depend on f_{NL} .

approximately describe the evolution of large-scale perturbations. In this case one writes [51, 55]

$$\delta^L = \sum_{j=1}^{\infty} a_j (\delta^E)^j, \quad (35)$$

where the a_j 's parameterize the evolution of mass-density fluctuations. For the simple case of spherical collapse, we have [65]

$$a_1 = 1; \quad a_2 = -17/21; \quad a_3 = 341/567. \quad (36)$$

Starting from the Lagrangian halo density perturbations δ_h^L given in Eq. (26) we want to use Eqs. (4) and (35) to write the Eulerian halo overdensity in terms of Eulerian density perturbations. This gives:

$$\begin{aligned} \delta_h(\mathbf{x}) = & b_0 + b_{10} \delta + b_{01} \varphi + \\ & + \frac{1}{2!} (b_{20} \delta^2 + 2 b_{11} \delta \varphi + b_{02} \varphi^2) + \\ & + \frac{1}{3!} (b_{30} \delta^3 + 3 b_{21} \delta^2 \varphi + 3 b_{12} \delta \varphi^2 + b_{03} \varphi^3), \end{aligned} \quad (37)$$

where all the density perturbations on the r.h.s. are Eulerian and non-Gaussian (from now on we drop the superscript E and all densities will be Eulerian unless explicitly stated otherwise) and the bias coefficients are given by the following expressions:

$$\begin{aligned} b_{10} &= 1 + a_1 b_{10}^L \\ b_{20} &= 2(a_1 + a_2) b_{10}^L + a_1^2 b_{20}^L \\ b_{30} &= 6(a_2 + a_3) b_{10}^L + 3(a_1^2 + 2a_1 a_2) b_{20}^L + a_1^3 b_{30}^L \\ b_{01} &= b_{01}^L \\ b_{11} &= b_{01}^L + a_1 b_{11}^L / 2 \\ b_{02} &= b_{02}^L \\ b_{21} &= (a_1 + a_2) b_{11}^L + a_1^2 b_{21}^L / 3 \\ b_{12} &= b_{02}^L + a_1 b_{12}^L / 3 \\ b_{03} &= b_{03}^L. \end{aligned} \quad (38)$$

$q_{10} = b_{10}$	$q_{11} = b_{01}$	$q_{22} = b_{11}/2$	$q_{23} = b_{02}/2$			
$q_{20} = b_{10}$	$q_{21} = b_{20}/2$	$q_{32} = b_{11}/2$	$q_{33} = b_{21}/6$	$q_{34} = b_{12}/6$	$q_{35} = b_{30}/6$	$q_{36} = b_{03}/6$
$q_{30} = b_{10}$	$q_{31} = b_{20}$					

TABLE I: Mapping of the bias coefficients in the full perturbative expansion.

Note that Eq. (37) differs from Eq. (2) due to the presence of extra terms which are proportional to different powers of the Gaussian auxiliary potential φ . Since φ is nearly scale invariant while δ has a larger variance on smaller scales, the additional terms will only affect the statistics of the halo distribution on the largest scales. Also, φ does not evolve with time while δ does (according to $\delta(z) = D(z)\delta(z=0)$ at linear order) thus implying that, for a given set of bias coefficients, the new terms will become less and less important over time. A third peculiarity of Eq. (37) is that the halo overdensity can differ from zero also in regions with mean mass density.

E. Perturbative expansion

In order to account for the non-linear evolution of mass-density fluctuations in Eq. (37) we use standard Eulerian perturbation theory (see [65] for a review). We therefore expand the density fields to third order as $\delta = \delta_1 + \delta_2 + \delta_3 + \mathcal{O}(\delta_4)$ where δ_n is $\mathcal{O}(\delta_1^n)$. Each term can be expressed as

$$\tilde{\delta}_n(\mathbf{k}) = \int \frac{d^3 \mathbf{q}_1}{(2\pi)^3} \cdots \frac{d^3 \mathbf{q}_n}{(2\pi)^3} \delta_D \left(\mathbf{k} - \sum_{i=1}^n \mathbf{q}_i \right) J_n(\mathbf{q}_1, \dots, \mathbf{q}_n) \tilde{\delta}_1(\mathbf{q}_1) \cdots \tilde{\delta}_1(\mathbf{q}_n), \quad (39)$$

where δ_D is the Dirac delta distribution, the tilde denotes Fourier transformation, and the J_n are specific kernel functions. On the other hand, since the Gaussian potential φ is the primordial one, there is no need to expand it, and it fully coincides with its first-order part $\varphi \equiv \varphi_1$.

We can now explicitly rewrite Eq. (37) up to the third perturbative order as

$$\begin{aligned} \delta_h(\mathbf{x}) &= b_0 + q_{10}\delta_1 + q_{11}\varphi_1 + \\ &+ q_{20}\delta_2 + q_{21}\delta_1^2 + q_{22}\delta_1\varphi_1 + q_{23}\varphi_1^2 + \\ &+ q_{30}\delta_3 + q_{31}\delta_1\delta_2 + q_{32}\delta_2\varphi_1 + q_{33}\delta_1^2\varphi_1 + q_{34}\delta_1\varphi_1^2 + q_{35}\delta_1^3 + q_{36}\varphi_1^3, \end{aligned} \quad (40)$$

where, to simplify the notation and facilitate bookkeeping of the terms which will appear in the perturbative expression for the power spectrum, we have replaced the biases b_{ij} with new coefficients q_{ij} . The explicit form of these is given in Table I.

Eq. (40) fully describes the Eulerian halo bias at the third perturbative order in the non-Gaussian case. The leading order term, $\delta_h \simeq [1 + a_1 b_{10}^L(f_{\text{NL}})] \delta + 2f_{\text{NL}} b_{10}^L(f_{\text{NL}}) \varphi$, was already recognized by Dal07, [37] and [36].

V. CLUSTERING STATISTICS AND NON-GAUSSIANITY

Statistical analysis of random fields, such as the Bardeen potential $\Phi(\mathbf{x})$, can be performed by studying the irreducible N -point correlation functions $\langle \Phi(\mathbf{x}_1)\Phi(\mathbf{x}_2)\dots\Phi(\mathbf{x}_N) \rangle$, or alternatively the N -spectra

$$(2\pi)^3 \mathcal{S}_N(\mathbf{k}_1, \mathbf{k}_2, \dots, \mathbf{k}_N) \delta_D(\mathbf{k}_1 + \mathbf{k}_2 + \dots + \mathbf{k}_N) = \langle \tilde{\Phi}(\mathbf{k}_1)\tilde{\Phi}(\mathbf{k}_2)\dots\tilde{\Phi}(\mathbf{k}_N) \rangle. \quad (41)$$

For Gaussian fields all odd-order spectra vanish. On the other hand, thanks to Wick's theorem, the reducible even-order correlators can be decomposed as products of the power spectrum,

$$(2\pi)^3 P_\Phi(k) \delta_D(\mathbf{k}_1 + \mathbf{k}_2) = \langle \tilde{\Phi}(\mathbf{k}_1)\tilde{\Phi}(\mathbf{k}_2) \rangle, \quad (42)$$

which, in this case, encodes all the information. If some non-Gaussianity is instead introduced, then higher-order statistics become important, such as the bispectrum

$$(2\pi)^3 B_\Phi(\mathbf{k}_1, \mathbf{k}_2, \mathbf{k}_3) \delta_D(\mathbf{k}_1 + \mathbf{k}_2 + \mathbf{k}_3) = \langle \tilde{\Phi}(\mathbf{k}_1)\tilde{\Phi}(\mathbf{k}_2)\tilde{\Phi}(\mathbf{k}_3) \rangle, \quad (43)$$

and the irreducible trispectrum

$$(2\pi)^3 T_\Phi(\mathbf{k}_1, \mathbf{k}_2, \mathbf{k}_3, \mathbf{k}_4) \delta_D(\mathbf{k}_1 + \mathbf{k}_2 + \mathbf{k}_3 + \mathbf{k}_4) = \langle \tilde{\Phi}(\mathbf{k}_1)\tilde{\Phi}(\mathbf{k}_2)\tilde{\Phi}(\mathbf{k}_3)\tilde{\Phi}(\mathbf{k}_4) \rangle. \quad (44)$$

Using our simplest model of non-Gaussianity given in Eq. (9) to define the non-Gaussian potential Φ in terms of the Gaussian one φ , we obtain:

$$P_{\Phi}(k) = P_{\varphi}(k) + 2f_{\text{NL}}^2 \int \frac{d^3\mathbf{q}}{(2\pi)^3} P_{\varphi}(q) P_{\varphi}(|\mathbf{k} - \mathbf{q}|) \simeq P_{\varphi}(k) \quad (45)$$

$$B_{\Phi}(\mathbf{k}_1, \mathbf{k}_2, \mathbf{k}_3) \simeq 2f_{\text{NL}} [P_{\varphi}(k_1)P_{\varphi}(k_2) + (2 \text{ cyclic})] \quad (46)$$

$$T_{\Phi}(\mathbf{k}_1, \mathbf{k}_2, \mathbf{k}_3, \mathbf{k}_4) \simeq 4f_{\text{NL}}^2 \{P_{\varphi}(k_1)P_{\varphi}(k_2)[P_{\varphi}(|\mathbf{k}_1 + \mathbf{k}_3|) + P_{\varphi}(|\mathbf{k}_1 + \mathbf{k}_4|)] + (5 \text{ cyclic})\} \quad (47)$$

where we dropped a sub-leading term proportional to f_{NL}^N for each of the N -spectra (this is why we used the symbol of approximate equality).[‡] We have checked that the discarded terms are indeed negligibly small. For instance, the sub-leading contribution to P_{Φ} contributes less than 1% of the total for $|f_{\text{NL}}| \sim 1000$ in the k -range of interest.

Considering also the third-order term in Eq. (1) introduces additional contributions to the power spectrum of the Bardeen's potential. The leading-order term can be written as:

$$\Delta P_{\Phi}(k) = 6g_{\text{NL}}P_{\varphi}(k) \int \frac{d^3\mathbf{q}}{(2\pi)^3} P_{\varphi}(q). \quad (48)$$

For $P_{\varphi}(k) \propto k^{n_s-4}$, the integral above presents an ultraviolet ($k \rightarrow \infty$) divergence if $n_s \geq 1$ and an infrared ($k \rightarrow 0$) divergence if $n_s \leq 1$. In general, this is not a problem as the physical process creating the fluctuations will automatically introduce cutoffs in P_{φ} at small and large wavelengths. For example, cosmic inflation will generate perturbations with characteristic sizes comprised between the reheating scale and the present-day horizon [32]. However, if ΔP_{Φ} is non-negligible with respect to the leading-order contribution P_{φ} (i.e. if $6|g_{\text{NL}}|\langle\varphi^2\rangle$ is not much less than unity), the results of the perturbative expansion are of limited use unless artificial cutoffs are introduced and the parameters of the theory are renormalized. The condition above reduces to $|g_{\text{NL}}| \ll 10^7$ if the currently favored values for the amplitude and the spectral index of primordial perturbations are plugged in. Present-day observational limits on g_{NL} [29, 39] therefore suggests that ΔP_{Φ} should contribute at the percent level or less to the power spectrum of the potential. Note that in numerical simulations [39], non-physical infrared and ultraviolet cutoffs are introduced by the use of a finite volume with periodic boundary conditions. Considering a non-vanishing g_{NL} also adds another leading-order correction to the trispectrum of the Bardeen potential:

$$\Delta T_{\Phi}(\mathbf{k}_1, \mathbf{k}_2, \mathbf{k}_3, \mathbf{k}_4) \simeq 6g_{\text{NL}}P_{\varphi}(k_1)P_{\varphi}(k_2)P_{\varphi}(k_3) + (3 \text{ cyclic}), \quad (49)$$

while it does not modify the bispectrum of Φ at leading order.

Linear perturbations in the density at redshift z are related to those in the primordial potential (formally at $z \rightarrow \infty$) by the Poisson equation

$$\tilde{\delta}_1(k) = \alpha(k)\tilde{\Phi}(k) \quad (50)$$

with

$$\alpha(k) = \frac{2c^2k^2T(k)D(z)}{3\Omega_m H_0^2} \frac{g(0)}{g(\infty)}, \quad (51)$$

where the matter growth factor $D(z)$ and the transfer function $T(k)$ have been introduced to account for the linear evolution of δ_1 . The function $g(z) \equiv (1+z)D(z)$ is the linear growth factor for the potential, and $g(\infty)/g(0) \simeq 1.3$ in the currently favored cosmology. Therefore, we can relate the power spectrum of linear density fluctuations to the power spectrum of the primordial potential by writing

$$P_0(k) \equiv P_{\delta_1}(k) = \alpha^2(k)P_{\Phi}(k) \simeq \alpha^2(k)P_{\varphi}(k), \quad (52)$$

where the last approximation follows from Eq. (45). Similar equations can be written for the three- and four-point correlators of the linear density perturbations, which we will label B_0 and T_0 respectively, by combining Eq. (50) with Eq. (46) and (47).

[‡] In multi-field inflationary models the non-Gaussian contribution to the trispectrum may scale independently from the bispectrum. For this reason, the factor f_{NL}^2 in Eq. (47) is sometimes re-labeled τ_{NL} , and treated as an independent parameter. Observational constraints on the trispectrum of the Bardeen's potential should then discriminate between such models and the simplest inflationary scenarios.

The fact that the Bardeen's potential decays with time proportionally to $g(z)$ implies that the actual values of the coefficients $Q_{\text{NL}j}$ depend on the cosmic epoch at which Eq. (1) is applied (see Section 2.2 in [41]). Here we apply it at early times (which is sometimes called the ‘‘CMB convention’’) while other authors use the fields linearly extrapolated at $z = 0$ (the ‘‘LSS convention’’). In general,

$$Q_{\text{NL}j}^{\text{LSS}} = Q_{\text{NL}j}^{\text{CMB}} \left[\frac{g(\infty)}{g(0)} \right]^j \quad (53)$$

so that $f_{\text{NL}}^{\text{LSS}} \simeq 1.3 f_{\text{NL}}^{\text{CMB}}$ and $g_{\text{NL}}^{\text{LSS}} \simeq 1.7 g_{\text{NL}}^{\text{CMB}}$. This conversion factors should be taken into account when comparing papers using different conventions.

VI. POWER SPECTRA

We are now ready to calculate the two-point statistics of the LSS arising from non-Gaussian initial conditions. We compute the halo-halo power spectrum and the halo-matter cross spectrum as follows. First, we take the Fourier transform of Eq. (40) and build the corresponding two-point correlators $\langle \tilde{\delta}_h(\mathbf{k}_1) \tilde{\delta}_h(\mathbf{k}_2) \rangle$ and $\langle \tilde{\delta}_h(\mathbf{k}_1) \tilde{\delta}(\mathbf{k}_2) \rangle$. These are composed of many pieces and we only consider terms up to the fourth perturbative order. For instance the leading contribution to halo-halo spectrum (second order in terms of the perturbations) is composed of 3 terms, the third order correction is made of 8 pieces (of which one identically vanishes because φ is a Gaussian field), and the fourth-order one contains 30 terms (14 of which are obtained multiplying a linear perturbation by a third-order one – indicated by the subscript $_{(13)}$ hereafter – and 16 are originated by the product of two second-order terms – subscript $_{(22)}$ hereafter). To proceed we then: (a) use Eq. (39) and write the density perturbations of order $n > 1$ as convolutions of n linear perturbations and a kernel J_n ; (b) express the linear density perturbations in terms of the potential Φ using the Poisson Eq. (50); (c) take the ensemble averages by using the expressions for the power spectrum, bispectrum and trispectrum given in Eqs. (46), (47), (49), and (52). While $\langle \tilde{\varphi}(\mathbf{k}_1) \tilde{\varphi}(\mathbf{k}_2) \tilde{\varphi}(\mathbf{k}_3) \rangle = 0$, attention must be paid to the mixed terms in Φ and φ as:

$$\langle \tilde{\Phi}(\mathbf{k}_1) \tilde{\Phi}(\mathbf{k}_2) \tilde{\Phi}(\mathbf{k}_3) \rangle \simeq \langle \tilde{\varphi}(\mathbf{k}_1) \tilde{\Phi}(\mathbf{k}_2) \tilde{\Phi}(\mathbf{k}_3) \rangle + (2 \text{ cyc.}) \simeq \langle \tilde{\varphi}(\mathbf{k}_1) \tilde{\varphi}(\mathbf{k}_2) \tilde{\Phi}(\mathbf{k}_3) \rangle + (2 \text{ cyc.}) \propto f_{\text{NL}} \quad (54)$$

where equalities only hold at leading order in φ^n (i.e. φ^4) as the central correlator also contains a sub-leading term proportional to $f_{\text{NL}} g_{\text{NL}}$ (which scales as φ^6) and the leftmost one some terms proportional to f_{NL}^3 , $f_{\text{NL}} g_{\text{NL}}$ (both scaling as φ^6), and $f_{\text{NL}} g_{\text{NL}}^2$ ($\propto \varphi^8$). Similarly, to leading order in φ^n (i.e. φ^6),

$$\langle \tilde{\Phi}(\mathbf{k}_1) \tilde{\Phi}(\mathbf{k}_2) \tilde{\Phi}(\mathbf{k}_3) \tilde{\Phi}(\mathbf{k}_4) \rangle \simeq f_{\text{NL}}^2 T_A + g_{\text{NL}} T_B \quad (55)$$

$$\langle \tilde{\varphi}(\mathbf{k}_1) \tilde{\Phi}(\mathbf{k}_2) \tilde{\Phi}(\mathbf{k}_3) \tilde{\Phi}(\mathbf{k}_4) \rangle + (3 \text{ cyc.}) \simeq 2 f_{\text{NL}}^2 T_A + 3 g_{\text{NL}} T_B \quad (56)$$

$$\langle \tilde{\varphi}(\mathbf{k}_1) \tilde{\varphi}(\mathbf{k}_2) \tilde{\Phi}(\mathbf{k}_3) \tilde{\Phi}(\mathbf{k}_4) \rangle + (5 \text{ cyc.}) \simeq f_{\text{NL}}^2 T_A + 3 g_{\text{NL}} T_B \quad (57)$$

$$\langle \tilde{\varphi}(\mathbf{k}_1) \tilde{\varphi}(\mathbf{k}_2) \tilde{\varphi}(\mathbf{k}_3) \tilde{\Phi}(\mathbf{k}_4) \rangle + (3 \text{ cyc.}) \simeq g_{\text{NL}} T_B \quad (58)$$

where $T_A(\mathbf{k}_1, \mathbf{k}_2, \mathbf{k}_3, \mathbf{k}_4)$ and $T_B(\mathbf{k}_1, \mathbf{k}_2, \mathbf{k}_3, \mathbf{k}_4)$ are defined in Eqs. (47) and (49).

A. Results and comparison with N-body simulations

Matter If we set $b_{10} = 1$ and all the other bias coefficients to zero, we obtain an expression for the power spectrum of mass-density perturbations which coincides with the result by [43]: $P^{mm}(k, z) = D^2(z) P_{11}(k) + D^3(z) P_{12}^{mm}(k) + D^4(z) [P_{22}^{mm}(k) + P_{13}^{mm}(k)]$, where

$$\begin{aligned} P_{11}^{mm}(k) &= P_0(k) \\ P_{12}^{mm}(k) &= 2 \int \frac{d^3 \mathbf{q}}{(2\pi)^3} J_2^{(s)}(\mathbf{q}, \mathbf{k} - \mathbf{q}) B_0(-\mathbf{k}, \mathbf{q}, \mathbf{k} - \mathbf{q}) \\ P_{22}^{mm}(k) &= 2 \int \frac{d^3 \mathbf{q}}{(2\pi)^3} \left[J_2^{(s)}(\mathbf{q}, \mathbf{k} - \mathbf{q}) \right]^2 P_0(q) P_0(|\mathbf{k} - \mathbf{q}|) + \\ &\quad + \int \frac{d^3 \mathbf{p} d^3 \mathbf{q}}{(2\pi)^6} J_2^{(s)}(\mathbf{p}, \mathbf{k} - \mathbf{p}) J_2^{(s)}(\mathbf{q}, -\mathbf{k} - \mathbf{q}) T_0(\mathbf{p}, \mathbf{k} - \mathbf{p}, \mathbf{q}, -\mathbf{k} - \mathbf{q}) \end{aligned}$$

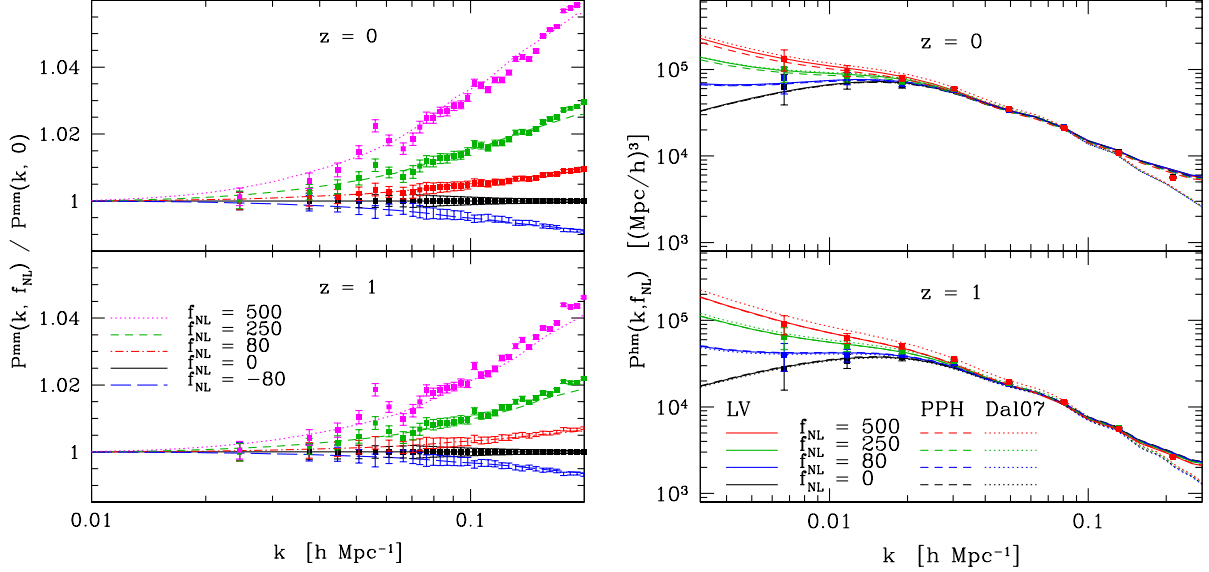


FIG. 3: **Left:** Deviation of the matter power spectrum in models with different f_{NL} (and $g_{NL} = 0$) from the Gaussian case at $z = 0$ (top) and $z = 1$ (bottom). The lines indicate our one-loop calculation for different values of f_{NL} while points with error bars correspond to the N-body simulations by PPH08. **Right:** Halo-matter cross spectrum at $z = 0$ for a narrow bin of halo masses centered around $M = 2 \cdot 10^{14} M_{\odot}/h$ (top) and at $z = 1$ for $M = 5 \cdot 10^{13} M_{\odot}/h$ (bottom). The solid and dashed lines have been obtained using our model with the bias parameters from the LV and PPH mass functions, respectively. The dotted lines indicate the model by Dal07, while points with error bars correspond to the simulations by PPH08.

$$\begin{aligned}
 P_{13}^{mm}(k) = & 6 \int \frac{d^3 \mathbf{q}}{(2\pi)^3} J_3^{(s)}(\mathbf{k}, \mathbf{q}, -\mathbf{q}) P_0(q) P_0(k) + \\
 & + 2 \int \frac{d^3 \mathbf{p} d^3 \mathbf{q}}{(2\pi)^6} J_3^{(s)}(\mathbf{p}, \mathbf{q}, \mathbf{k} - \mathbf{p} - \mathbf{q}) T_0(-\mathbf{k}, \mathbf{p}, \mathbf{q}, \mathbf{k} - \mathbf{p} - \mathbf{q}),
 \end{aligned} \tag{59}$$

and $J_n^{(s)}$ indicates a kernel which has been symmetrized with respect to its arguments. We have checked that the two-loop contributions proportional to T_0 are, in general, negligibly small and will not be considered hereafter if $g_{NL} = 0$. In the left panel of Fig. 3 we plot the ratio between the matter power spectra originating from a non-Gaussian model (with $f_{NL} \neq 0$ and $g_{NL} = 0$) and from Gaussian initial conditions. We consider several values of f_{NL} and we compare our analytical results with data from the N-body simulations by PPH08 at both redshift 0 and 1. Primordial non-Gaussianity alters the matter power spectrum at the few percent level for $k < 0.2 h \text{ Mpc}^{-1}$ and these deviations are remarkably well reproduced by the one-loop corrections.

Halos The halo-halo power spectrum (and similarly the halo-matter cross spectrum) deriving from our multivariate biasing scheme can be written as

$$P^{hj}(k, z) = D^2(z) P_{11}^{hj}(k) + D^3(z) P_{12}^{hj}(k) + D^4(z) \left[P_{22}^{hj}(k) + P_{13}^{hj}(k) \right], \tag{60}$$

where the superscript j indicates either matter (m) or halo (h) fluctuations. The full expressions of the different terms are lengthy and we report them only in the Appendix. We highlight that our calculation reduces to: (a) the linear result by Dal07 if we only consider the leading-order terms (and further assume that the mass function does not depend on f_{NL}); (b) the usual one-loop Gaussian expression derived e.g. by [57] if we set $f_{NL} = 0$, and (c) the non-Gaussian result by [43] if we ignore the terms which are proportional to the potential perturbations φ in our multivariate biasing scheme. Notice that for $k \rightarrow 0$ we obtain $P^{hh}(k) \propto P_0(k)/\alpha^2(k)$ and $P^{hm}(k) \propto P_0(k)/\alpha(k)$. In the right panel of Fig. 3, we test our theoretical predictions for the halo-matter cross spectrum as a function of f_{NL} and for $g_{NL} = 0$ (solid lines) against the N-body data by PPH08. The bias factors in the models have been calculated from the LV and PPH mass functions. We consider halos with mass $M \simeq 2 \cdot 10^{14} M_{\odot}/h$ at $z = 0$ and $M \simeq 5 \cdot 10^{13} M_{\odot}/h$ at $z = 1$. We have chosen two different mass bins to keep the number of halos at each redshift large enough to avoid substantial shot noise contamination in the simulations. Our analytical results are in very good agreement with the simulation data for the whole range of f_{NL} and up to scales $k \lesssim 0.2 h \text{ Mpc}^{-1}$. Note that our

spectra differ from the linear result by Dal07 (over-plotted with dotted lines) both on large and small scales. The small-scale departure is due to the non-linear growth of perturbations which we take into account up to the third perturbative order. The large-scale discrepancy is discussed in detail in the next subsection. In Fig. 4 we show how the cross spectrum depends on the halo mass at three different wavenumbers and for two redshifts. Independently of halo mass, at $z = 1$ our model accurately matches the outcome of the simulations for $k < 0.2 h \text{ Mpc}^{-1}$. Likewise, at $z = 0$, the theory agrees well with the numerical data on the largest scales while it tends to over-predict the cross power for $k > 0.1 h \text{ Mpc}^{-1}$ and $M < 10^{14} M_\odot/h$.

We have checked that, for $g_{\text{NL}} = 0$, the terms proportional to the trispectra of the potentials Φ and φ are generally subdominant even when they generate contributions to the halo power spectrum which diverge as $k \rightarrow 0$. For instance, the trispectrum contribution to the term $\langle \widetilde{\delta}_1^2 \widetilde{\delta}_1^2 \rangle$ in the halo-halo power spectrum scales as $P_0(k)/\alpha^2(k)$ as like as the leading term. However, for $|f_{\text{NL}}| < 500$, this correction contributes at most at percent level and only on very large scales. Also the trispectrum contribution in $\langle \widetilde{\delta}_1^3 \widetilde{\delta}_1 \rangle$ which scales as $P_0(k)/\alpha(k)$ is subdominant ($\ll 1\%$) for both the halo-halo and the halo-matter cases. Similar conclusions can be drawn for the terms including φ : we have checked that the contributions arising from averages where one or more δ_1 are replaced by φ are subdominant.

The effect of g_{NL} The situation becomes more complicated if we consider also the third-order term in Eq. (1) with realistic values of g_{NL} . In this case, there will be new contributions to the halo and halo-matter power spectra coming from two sources: the trispectrum gets the additional term of Eq. (49), and the bias factors become altered as described in Eq. (31); each of these modifications is linear in g_{NL} .

Considering first the effect of ΔT_Φ , we have found that this adds a (negligible) constant contribution to $\langle \widetilde{\delta}_1^2 \widetilde{\delta}_1^2 \rangle$ but generates another term which scales as $P_0(k)/\alpha(k)$ in $\langle \widetilde{\delta}_1^3 \widetilde{\delta}_1^3 \rangle$. The latter can become the dominant contribution on large scales and for high values of $g_{\text{NL}} \gtrsim 10^5$. In the limit $k \rightarrow 0$, this two-loop term (whose full expression is given in Eqs. (82,88) in the Appendix for the halo and halo-matter cases) reduces to

$$\begin{aligned} P_{13}^{hh,II}(k) &\rightarrow g_{\text{NL}} b_{10} b_{30} \sigma^4(R) \Sigma_3(R) \frac{P_0(k)}{\alpha(k)} \propto g_{\text{NL}} k^{n_s-2} \\ P_{13}^{hm,II}(k) &\rightarrow \frac{1}{2} g_{\text{NL}} b_{30} \sigma^4(R) \Sigma_3(R) \frac{P_0(k)}{\alpha(k)} \propto g_{\text{NL}} k^{n_s-2}, \end{aligned} \quad (61)$$

where we define

$$\Sigma_3(R) \equiv \int \frac{d^3 \mathbf{p} d^3 \mathbf{q}}{(2\pi)^6} \frac{P_0(q)}{\alpha(q)} \frac{P_0(p)}{\alpha(p)} \alpha(|\mathbf{p} + \mathbf{q}|) W(qR) W(pR), \quad (62)$$

such that $S_3 = f_{\text{NL}} \Sigma_3$. In our formalism, $P_{13}^{hh,II}(k)$ corresponds to the leading contribution found by [39], who used it to derive observational constraints on g_{NL} (assuming $f_{\text{NL}} = 0$). In the limit of high peaks, the scaling $b_{10} b_{30} \rightarrow (\delta_c/\sigma)^4$ is recovered. Note, however, that the amplitude of this term depends on the adopted smoothing scale R first introduced in Section II, and further discussed in Section VI C.

Second, we look at the effect of Δb . As shown in Eq. (31), only the coefficients b_{02} and b_{12} are altered by g_{NL} . In the halo-matter case these new terms are subdominant with respect to the trispectrum contribution of Eq. (61). However, in the halo-halo spectrum, the leading term for $k \rightarrow 0$ is $P_{(23)(23)}^{hh} \propto \langle \widetilde{\varphi}^2 \widetilde{\varphi}^2 \rangle \propto b_{02}^2$, which scales as

$$P_{(23)(23)}^{hh} \rightarrow \frac{1}{2} b_{02}^2 \sigma_\varphi^2(R) \frac{P_0(k)}{\alpha^2(k)} \propto g_{\text{NL}}^2 k^{n_s-4}, \quad (63)$$

where $\sigma_\varphi^2 = \int dq q^2 [P_0(q)/\alpha^2(q)] W^2(qR)/(2\pi^2)$. Because of the quadratic dependence on g_{NL} , this term dominates on very large scales for high values of g_{NL} and small f_{NL} . Its dependence on the smoothing radius R is very weak because the potential φ is nearly scale invariant. Note that the terms in $f_{\text{NL}} g_{\text{NL}}$ are generally subdominant.

B. Bias and asymptotic behavior on large scales

Let us define the effective bias function

$$b_{\text{eff}}(k, f_{\text{NL}}) \equiv \frac{P^{hm}(k, f_{\text{NL}})}{P^{mm}(k, f_{\text{NL}})}, \quad (64)$$

and compare it with the standard Gaussian bias by introducing the bias deviation

$$\Delta b(k, f_{\text{NL}}) = b_{\text{eff}}(k, f_{\text{NL}}) - b_{\text{eff}}(k, 0). \quad (65)$$

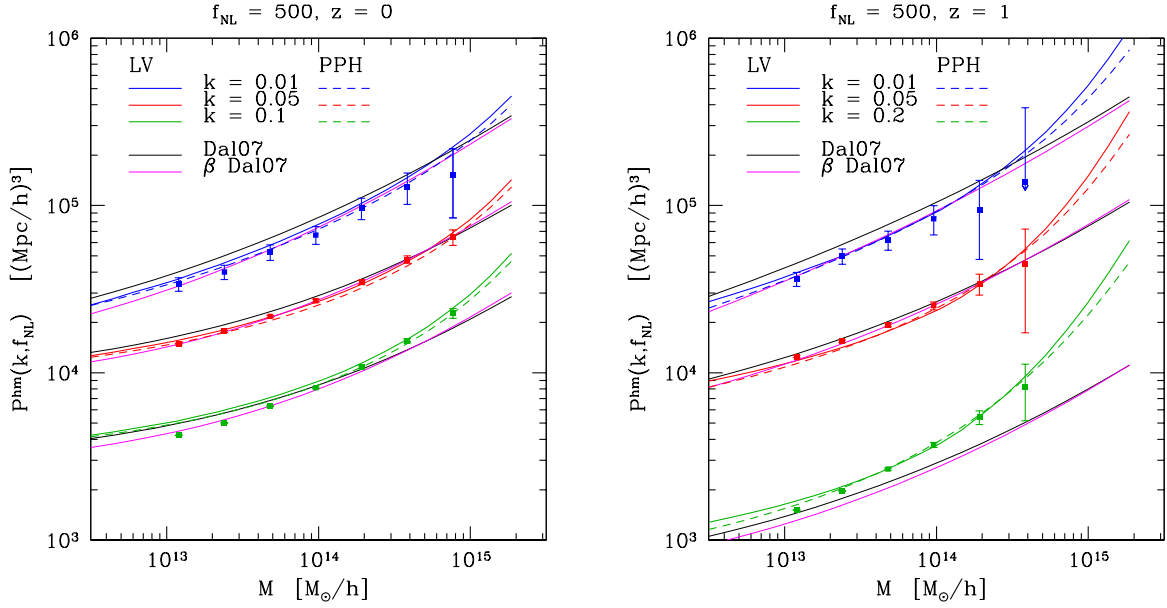


FIG. 4: The halo-matter cross spectrum as a function of halo mass at $z = 0$ (left) and $z = 1$ (right) is plotted for three different values of the comoving wavenumber k (in $h \text{ Mpc}^{-1}$). Colored solid and dashed lines indicate the results of our perturbative calculation using the LV and PPH mass functions, respectively. Data points with error bars correspond to the N-body simulations by PPH08. The thin lines show the linear theory by Dal07 (black), also corrected with the factor β (magenta) introduced by PPH08 (see Section VIB for further details). At $z = 0$ structure has evolved further into the non-linear regime, so that the range of validity of both the linear and one loop theories is reduced.

In this section we will only consider the case $g_{\text{NL}} = 0$. In the limit $k \rightarrow 0$ and for large R ($\sigma_R^2 \ll 1$), the dominant contribution to the halo power spectrum is given by the tree-level term, and we thus obtain

$$\Delta b_{\text{linear}}(k) = b_{10}(f_{\text{NL}}) - b_{10}(f_{\text{NL}} = 0) + 2f_{\text{NL}}\delta_c [b_{10}(f_{\text{NL}}) - 1]/\alpha(k). \quad (66)$$

The scale-dependent non-Gaussian correction is proportional to the factor $b_{10} - 1$ as originally shown by Dal07, although there is also an additional scale-independent correction, due to the fact that in our model b_{10} is a function of f_{NL} (similar conclusions have been reached by [36, 38–41] following different approaches). In the simplest model by Dal07 the scale-independent term is missing:

$$\Delta b_{\text{Dal07}}(k) = 2f_{\text{NL}}\delta_c [b_{10}(f_{\text{NL}}) - 1]/\alpha(k). \quad (67)$$

In the left panel of Fig. 5, we plot $\Delta b(k)$ for $f_{\text{NL}} = 500$ and test the different models against the N-body simulations by PPH08. We can see that considering only the scale-dependent term as in Dal07 does not match the simulations very well, since, contrary to the N-body data, Δb cannot change sign with increasing k (see also [41]). The agreement vastly improves if we use Eq. (66) with the bias parameters computed from a non-Gaussian mass function (LV) as this adds a constant negative shift (see the left panel of Fig. 2) to the bias deviation. Considering the full calculation to third perturbative order further improves the agreement with the simulations for $k > 0.1 h \text{ Mpc}^{-1}$ up to a maximum value of the wavenumber which depends on the adopted smoothing scale for the perturbative calculations (see Section VIC for further details). To highlight the importance of the non-linear and scale-independent corrections, in the right panel of Fig. 5 we plot the ratio

$$\frac{\Delta b(k, f_{\text{NL}})}{\Delta b_{\text{Dal07}}(k, f_{\text{NL}})} \quad (68)$$

for several values of f_{NL} and using both the LV and PPH mass functions. We consider halos with mass $M = 2 \cdot 10^{14} h^{-1} M_{\odot}$ at $z = 0$. The simulation data by PPH08 are in good agreement with our third-order calculation, while the linear (Dal07) model cannot reproduce them on scales $k > 0.02 h \text{ Mpc}^{-1}$. The impact of primordial non-Gaussianity on the halo bias is further explored in the left panel of Fig. 6, where we show the bias deviation as a function of f_{NL} at three selected scales, again for halos with $M = 2 \cdot 10^{14} h^{-1} M_{\odot}$ at $z = 0$. Note that, contrary to

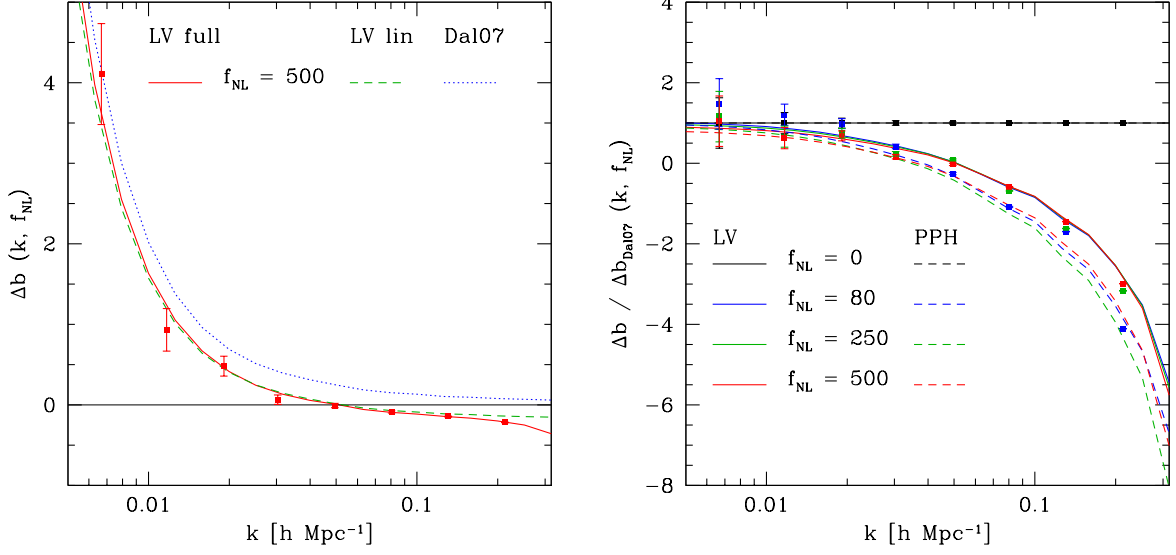


FIG. 5: **Left:** Change in the effective bias Δb for fixed $f_{\text{NL}} = 500$, $M = 2 \cdot 10^{14} M_{\odot}/h$, at $z = 0$. Different models are compared with N-body simulations: the simple Δb_{Dal07} (dotted), Δb_{linear} (dashed) using the LV mass function, and the full one-loop theory (solid), which yields the best match. **Right:** Fractional difference between the one-loop prediction for Δb (with LV and PPH mass functions) and the Dal07 linear theory, compared with the simulations, for different values of f_{NL} , at the same mass and redshift.

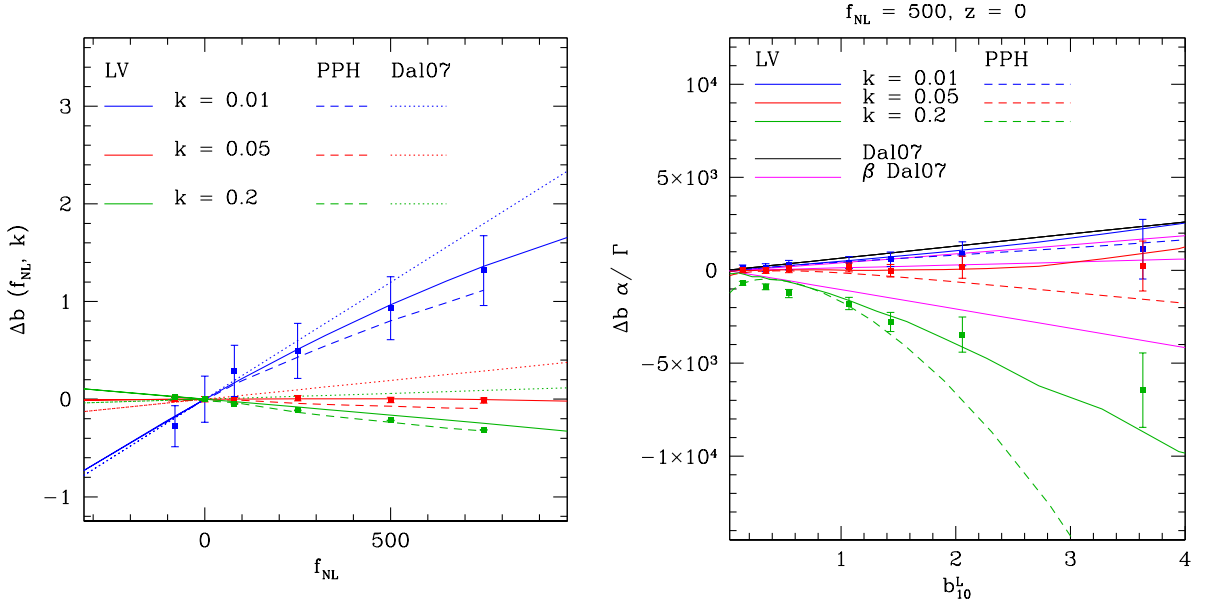


FIG. 6: **Left:** Bias deviation at $z = 0$ as a function of f_{NL} at three different wavenumbers, and for $M = 2 \cdot 10^{14} M_{\odot}/h$. The results for LV (solid) and PPH (dashed, within its range of validity) mass functions are shown. We also plot the prediction for the linear (Dal07) theory. **Right:** As in the left panel but as a function of b_1^L and for $f_{\text{NL}} = 500$. The normalization factor $\alpha/\Gamma \equiv \alpha/(2A)$ is chosen to reproduce figure 11 in PPH08.

what predicted by the linear (Dal07) model, the relationship between Δb and f_{NL} is non-linear, as first observed by PPH08 in their N-body simulations, and this is now fully explained by our perturbative calculation to third order. We finally study the mass dependence of the bias deviation by showing, in the right panel of Fig. 6, how Δb changes as a function of the first Lagrangian bias coefficient b_{10}^L . We consider three values of the wavenumber in the quasi-linear and mildly non-linear regime, $f_{\text{NL}} = 500$, and $z = 0$. In the Dal07 model, Δb depends linearly on b_1^L and the relation between these two quantities is independent of k . This is indicated by the solid black line which departs more and more from the simulation data with increasing k . In order to better describe the N-body results, PPH08 presented a fitting function, $\beta(k, f_{\text{NL}})$, in the form of a multiplicative (scale-dependent) correction to the Dal07 model (magenta lines). Note that our third-order calculations match well the numerical outcome. Some discrepancy is noticeable for $k = 0.2 h \text{ Mpc}^{-1}$ and $b_{10}^L < 1$, where non-linear effects become more important (due to the small first bias coefficient) and perturbation theory becomes less accurate. The difference between the bias deviations obtained with the LV and PPH mass functions at large halo masses emphasize the need for accurate parameterizations of the halo counts for the rarest objects.

Our result in Eq. (66) differs from the perturbative calculations based on the univariate local bias by [43, 44] where the scale-dependent part of the bias deviation was found to scale as b_{20} times the variance of the mass density field. Strictly speaking, for $f_{\text{NL}} \neq 0$ and $k \rightarrow 0$ our result gives $P^{hm}(k, f_{\text{NL}}) \rightarrow (b_{01} + 2b_{20}f_{\text{NL}}\sigma_R^2)P_0(k)/\alpha(k)$ but the term proportional to b_{20} is suppressed by smoothing on the scale R (which is necessary to truncate the bias expansion at third order in a meaningful way). Note that, using the PS expression for the bias parameters in the limits of high peaks, $\delta_c/\sigma \gg 1$, this reduces to $P^{hm}(k, f_{\text{NL}}) \rightarrow 2f_{\text{NL}}(\delta_c^2/\sigma^2)[1 + (\sigma_R^2/\sigma^2)]P_0(k)/\alpha(k)$. In this case, the two contributions are identical if R is chosen to be the Lagrangian radius of the halos (i.e. $R = R_f$) and the same window function is used to compute σ and in the calculation of the perturbative power spectra. In general, however, using the Lagrangian radius of the halos gives σ of order unity and this is too large to allow the truncation of the bias expansion at a finite order. For this reason in our calculations we use $\sigma_R < \sigma$ and the smoothing-dependent contribution proportional to b_{20} is subdominant.[§]

As highlighted in Eq. (37) the leading order for δ_h in our multivariate biasing scheme includes a term proportional to φ and this generates the scale-dependent correction in Δb . The proportionality with b_{20} found by other authors derives from the assumption that a local deterministic bias scheme holds true also in the presence of non-Gaussian perturbations. In this case, for $k \rightarrow 0$, second-order terms dominate over the tree-level contribution to the power spectrum which casts some doubts on the validity of the perturbative expansion. In the left panel of Fig. 7 we show the difference between our multivariate approach and the standard local bias. The asymptotic scale dependence $P^{hm}(k) \propto \alpha^{-1}(k)P_0(k) \propto k^{n_s-2}$ for $k \rightarrow 0$ is recovered in both cases, but the amplitude of the diverging term in the standard local bias model depends on the smoothing length that has to be introduced to cure the ultraviolet divergence of the mass variance. In Fig. 7 we use a smoothing scale of $10 h^{-1} \text{ Mpc}$ for both models and the asymptotic term deriving from the standard local bias is strongly subdominant with respect to the correction given in Eq. (66). As discussed by [43], the result of the univariate local model depends strongly on the smoothing scale, as it is proportional to $\sigma^2(R)$. For instance, using $R = 2h^{-1}\text{Mpc}$ boosts the amplitude of the scale-dependent bias (see Fig. 7 (left)). This is why only the multivariate model can reproduce the results from N-body simulations by PPH08 without tuning additional parameters. The main practical advantage in this case is that the bias parameters can be predicted from a model for the mass function, while the results from the standard local bias can only be used after “renormalizing” the bias coefficients [66] and using them as fitting functions. However, even though one can play with the parameters of the theory to fit some data, one should not forget that the physical origin of the scale-dependent bias is that large-scale fluctuations in δ_h trace perturbations in φ and this is not accounted for by the standard local bias model. The differences between the models are further highlighted in the right panel of Fig. 7, where we plot the ratio of the halo-matter cross spectra obtained with different approximations with respect to our full non-Gaussian one-loop calculation, at $f_{\text{NL}} = 500$ and at $z = 0$ and 1. This figure summarizes all the conclusion we have reached in this section: (1) the univariate local biasing assumption yields the correct k -dependence but the wrong amplitude of the spectrum on large scales; (2) the linear approximation in Eq. (66) lacks small-scale power; (3) the simpler model by Dal07 also features a scale-independent offset in the effective bias. Similar results can be obtained for the halo-halo power spectrum, for which the asymptotic scale dependence is $P^{hh}(k) \propto \alpha^{-2}(k)P_0(k) \propto k^{n_s-4}$ for $k \rightarrow 0$.

[§] It is interesting to see what alternative approaches find regarding this discrepancy. For instance, Matarrese & Verde [35] computed the two-point correlation function of regions where the density exceeds a high threshold $\delta_c \gg \sigma$ and found that, for large separations, the non-Gaussian correction scales as $(\delta_c^3/\sigma^6)\xi_3(\mathbf{x}_1, \mathbf{x}_1, \mathbf{x}_2)$ with ξ_3 the three-point correlation function of the mass density. In Fourier space this coincides with the high-peak limit of our result but, provided that $\sigma^2 = \sigma_R^2$, it also matches the result by [43]. This happens because for high peaks both $\delta_c(b_{10}^L)^2$ and $b_{10}^L b_{20}^L$ are proportional to δ_c^3 . The same ambiguity applies to the higher-order calculations in Desjacques & Seljak [39].

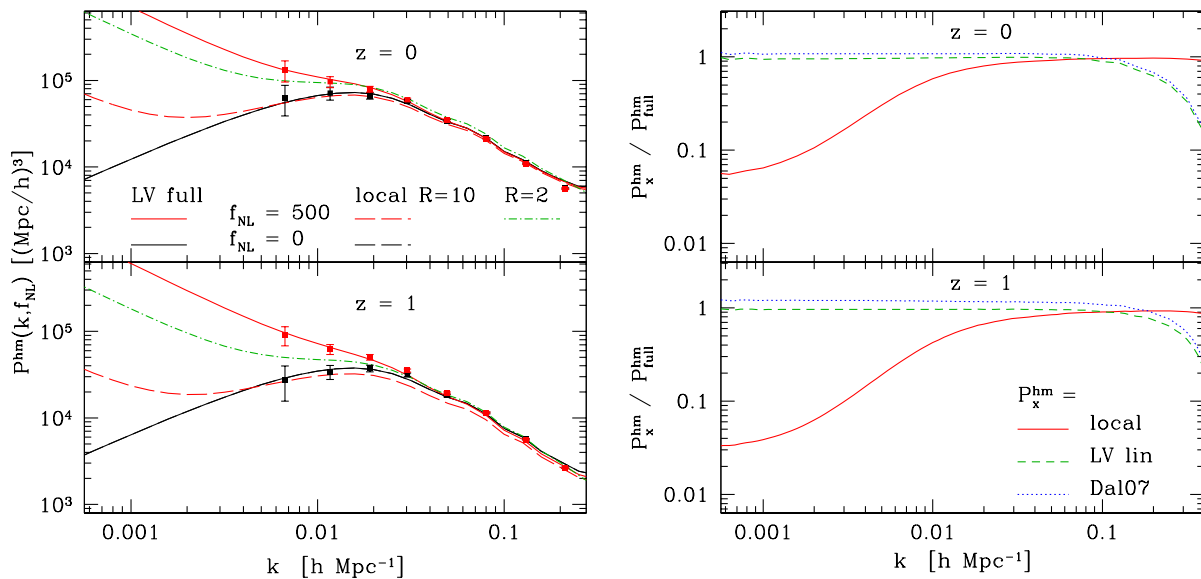


FIG. 7: **Left:** The standard univariate local bias prescription (local) is compared with our multivariate scheme for the halo bias (LV full). We consider the same halo masses as in Fig. 3 (right) and we plot the halo-matter cross spectra deriving from the two bias models at $z = 0, 1$ and with a smoothing scale $R = 10 h^{-1}$ Mpc. In the Gaussian case ($f_{NL} = 0$) the cross spectra coincide, but they are very different for $f_{NL} = 500$. While the asymptotic scale dependence for $k \rightarrow 0$ is recovered in both cases, only the multivariate model can reproduce the results from the N-body simulations. We also show the dependence on R in the univariate model, by overplotting the result with $R = 2 h^{-1}$ Mpc. **Right:** Ratio between the halo-matter cross spectra obtained with different approximations and our full perturbative calculation, using $f_{NL} = 500$ and for the same redshifts and halo masses as in Fig. 3. Assuming univariate local biasing (red, solid) severely under-predicts the large-scale power. On the other hand, the linear approximations in Eqs. (66) (green, dashed) and (67) (blue, dotted) lack small-scale power. Notice that the Dal07 model also features a constant offset on large scales due to the missing scale-independent correction discussed in the main text.

C. On the smoothing and other perturbative approaches

The series expansion in Eq. (2) only applies when δ_h and δ have been smoothed on a scale R . The reason is twofold. First, the locality of the bias is expected to degrade progressively when smaller and smaller scales are considered. Second, we truncate both the bias and the perturbative expansions to finite order which is a good approximation only if the neglected terms give a small contribution. This requires that typically $\delta \ll 1$, i.e. $R \gg 5 h^{-1}$ Mpc.

As explicitly indicated in the Appendix, in this paper we have used a Gaussian kernel $W(kR) = \exp[-(kR)^2/2]$ with $R = 10 h^{-1}$ Mpc to smooth the evolved fields δ_1 , δ_2 and δ_3 before applying Eq. (2). An obvious consequence of this procedure is that also the resulting halo power spectrum is suppressed on scales $k \gtrsim R^{-1}$. A common prescription to lessen this effect and extend the theory to (slightly) larger wavenumbers is to divide out $W^2(kR)$ from the perturbative result for $P^{hh}(k)$ and $P^{hm}(k)$, as introduced by [67]. Here we have followed this approach to consider wavenumbers up to $k \sim 0.3 h Mpc^{-1}$.

Some of the one-loop corrections to the halo power spectrum present ultraviolet divergences that are automatically cured by using a finite value of R . However, some of these integrals give rise to scale-independent contributions for $k \rightarrow 0$ whose amplitude depends on R , as shown already by [57]. This is somewhat unsatisfactory, since it makes the results dependent upon a non-fundamental quantity, and it is amongst the reasons which have led to the application of renormalization techniques to the theory, often borrowed from other areas of physics. The existing approaches, as recently reviewed by [68], include the renormalized perturbation theory [69, 70], the closure theory [71], the time renormalization group flow model [72], and the renormalization group perturbation theory [66, 73]. Most of these approaches do not include a bias model and just apply to the matter density field. The renormalization of the bias parameters, included in some of the models, makes the theory free from any undesired dependence on the smoothing scale. This can be achieved by grouping different perturbative terms together and relabeling some parameters to include the smoothing-dependent factors, a procedure which is not uniquely defined. An altogether different approach which does not need such an operation is the Lagrangian resummation theory by [56, 74].

On the other hand, SPT has the advantage of remaining a fully predictive theory, where the bias coefficients can be calculated as a function of halo mass. Furthermore, the choice of the smoothing scale R is not completely arbitrary, but confined to a rather narrow range around $R \simeq 10 h^{-1}$ Mpc. Indeed, the smoothing needs to be $R \gtrsim 8 h^{-1}$ Mpc in order not to break the validity of the perturbative expansion in a significant fraction of the volume ($\sigma \ll 1$ for matter and $\sigma \ll b_{20}/b_{10}$ for halos) and, on the other hand, R needs to be as close as possible to this limit if we want to prevent the smoothing from wiping out the non-linear corrections at the wavenumbers of interest.

We have checked numerically that different choices of the smoothing scale R within a reasonable range larger than the Lagrangian size of the halos do not affect our results significantly. Notice that, for non-Gaussian perturbations, the k -independent – but R -dependent – terms arising in SPT on large scales are less important, since the halo power spectrum grows with decreasing k .

VII. BISPECTRA

The leading contributions to the halo bispectrum from non-Gaussian initial conditions of the local type have been recently computed in the framework of the local bias model given in Eq. (2) [44–46]:

$$B_h(\mathbf{k}_1, \mathbf{k}_2, \mathbf{k}_3) = b_1^3 B_\delta(\mathbf{k}_1, \mathbf{k}_2, \mathbf{k}_3) + b_1^2 b_2 \left[P_\delta(k_1) P_\delta(k_2) + (2 \text{ cyc.}) + \frac{1}{2} \int \frac{d^3 q}{(2\pi)^3} T_\delta(\mathbf{q}, \mathbf{k}_1 - \mathbf{q}, \mathbf{k}_2, \mathbf{k}_3) + (2 \text{ cyc.}) \right]. \quad (69)$$

Using Eulerian perturbation theory to follow the growth of density perturbations gives up to fourth order

$$B_\delta(\mathbf{k}_1, \mathbf{k}_2, \mathbf{k}_3) \simeq B_0(\mathbf{k}_1, \mathbf{k}_2, \mathbf{k}_3) + 2F_2(\mathbf{k}_1, \mathbf{k}_2) P_0(k_1) P_0(k_2) + (2 \text{ cyc.}), \quad (70)$$

where the second term is generated by non-linear gravity while

$$B_0(\mathbf{k}_1, \mathbf{k}_2, \mathbf{k}_3) \simeq 2f_{\text{NL}} \left[\alpha(k_3) \frac{P_0(k_1) P_0(k_2)}{\alpha(k_1) \alpha(k_2)} + 2 \text{ cyc.} \right] \quad (71)$$

is the linear matter bispectrum due to primordial non-Gaussianity. Similarly, the term between square brackets in Eq. (69) reduces to

$$P_0(k_1) P_0(k_2) + (2 \text{ cyc.}) + \frac{1}{2} \int \frac{d^3 q}{(2\pi)^3} T_0(\mathbf{q}, \mathbf{k}_1 - \mathbf{q}, \mathbf{k}_2, \mathbf{k}_3) + (2 \text{ cyc.}). \quad (72)$$

In full analogy with the power spectrum calculation discussed above, it is straightforward to show that our new expansion of δ_h in terms of both δ and φ gives rise to many additional contributions. The most compact form is obtained by writing the expansion of the product of three δ_h evaluated in real space at three different locations. For the term which generates the contribution to the halo bispectrum which is proportional to the linear matter bispectrum, we have:

$$b_1 \delta_1 \delta_1 \delta_1 \rightarrow b_{10} \delta_1 \delta_1 \delta_1 + b_{10}^2 b_{01} \varphi \delta_1 \delta_1 + (2 \text{ cyc.}) + b_{10} b_{01}^2 \varphi \varphi \delta + (2 \text{ cyc.}) + b_{01}^3 \varphi \varphi \varphi. \quad (73)$$

On the other hand, for the term accounting for the non-linear evolution of the density, one finds:

$$b_1^3 \delta_1 \delta_1 \delta_2 + (2 \text{ cyc.}) \rightarrow b_{10}^3 \delta_1 \delta_1 \delta_2 + (2 \text{ cyc.}) + b_{10}^2 b_{01} \varphi \delta_1 \delta_2 + (5 \text{ cyc.}) + b_{10} b_{01}^2 \varphi \varphi \delta_2 + (2 \text{ cyc.}). \quad (74)$$

Finally, for the source of the term between square brackets in in Eq. (69), we get:

$$\begin{aligned} \frac{1}{2} b_1^2 b_2 \delta_1 \delta_1 \delta_1^2 + (2 \text{ cyc.}) &\rightarrow \frac{1}{2} b_{10}^2 b_{20} \delta_1 \delta_1 \delta_1^2 + (2 \text{ cyc.}) + b_{10}^2 b_{11} \delta_1 \delta_1 (\varphi \delta_1) + (2 \text{ cyc.}) + \frac{1}{2} b_{10} b_{20} b_{01} \delta_1 \varphi \delta_1^2 + (5 \text{ cyc.}) + \\ &\frac{1}{2} b_{10}^2 b_{02} \delta_1 \delta_1 \varphi^2 + (2 \text{ cyc.}) + b_{10} b_{01} b_{11} \delta_1 \varphi (\varphi \delta_1) + (5 \text{ cyc.}) + \frac{1}{2} b_{01}^2 b_{20} \varphi \varphi \delta_1^2 + (2 \text{ cyc.}) + \\ &\frac{1}{2} b_{10} b_{01} b_{02} \delta_1 \varphi \varphi^2 + (5 \text{ cyc.}) + b_{01}^2 b_{11} \varphi \varphi (\varphi \delta_1) + (2 \text{ cyc.}) + \frac{1}{2} b_{01}^2 b_{02} \varphi \varphi \varphi^2 + (2 \text{ cyc.}). \end{aligned} \quad (75)$$

The halo bispectrum can be computed by Fourier transforming the expressions above. For instance, from Eq. (73) we obtain:

$$B_h(\mathbf{k}_1, \mathbf{k}_2, \mathbf{k}_3) \simeq \left[b_{10} + \frac{b_{01}}{\alpha(k_1)} \right] \left[b_{10} + \frac{b_{01}}{\alpha(k_2)} \right] \left[b_{10} + \frac{b_{01}}{\alpha(k_3)} \right] B_0(\mathbf{k}_1, \mathbf{k}_2, \mathbf{k}_3), \quad (76)$$

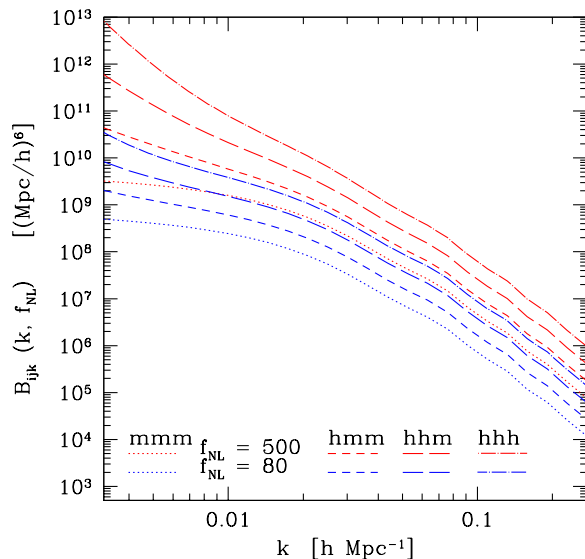


FIG. 8: Theoretical bispectra at tree level in the equilateral configuration: $B^{mmm}(k, k, k)$, $B^{hmm}(k, k, k)$, $B^{hhm}(k, k, k)$, $B^{hhh}(k, k, k)$ for two values of f_{NL} . In the Gaussian case ($f_{\text{NL}} = 0$) the tree-level bispectrum vanishes.

while assuming a local-bias scheme would have given $B_h(\mathbf{k}_1, \mathbf{k}_2, \mathbf{k}_3) \simeq b_{10}^3 B_0(\mathbf{k}_1, \mathbf{k}_2, \mathbf{k}_3)$. The mixed matter-halo bispectra can be obtained in a similar way, and their expressions differ from Eq. (76) only for the presence of a reduced number of scale-dependent bias factors. We plot the equilateral configuration of the bispectra in Fig. 8, for two values of f_{NL} . Since we are only considering the tree-level contribution, the Gaussian bispectrum is vanishing. Note that our leading-order result of Eq. (76) can be reproduced by taking the analogous formula obtained with the univariate local bias and simply replacing b_{10} with the scale-dependent bias $b_{10} + b_{01}/\alpha(k)$. More complex equations relate the scale-dependent terms obtained by taking the Fourier transform of Eqs. (74) and (75). We will not discuss them in detail here.

It is important to notice that the scale-dependent bias changes the shape dependence of the halo bispectrum. The tree-level term B_0 is dominated by the squeezed configurations (where one of the wavevectors is small) and the f_{NL} -dependent term b_{01}/α makes it even more so. Comparing our results with the figures in [46] suggests that, in strict analogy with the result for the power spectrum, the terms proportional to b_{01}/α give by far the dominant contribution to the bispectrum on large scales. The shapes of the bispectrum parts coming from the non-linear growth of perturbations and second-order biasing are very different [45, 46] and this makes the bispectrum a promising tool to measure f_{NL} .

We can see that the expanded form of the bispectrum deriving from Eqs. (74) and (75) depends on all the non-Gaussianity parameters in a non-trivial way: all terms involving the matter bispectrum B_0 , i.e. all terms involving an average over three δ 's or φ 's bring in a linear dependence on f_{NL} . Then, all terms involving the matter trispectrum T_0 , i.e. averages over four δ 's or φ 's, have two contributions, depending on g_{NL} and f_{NL}^2 (or in general τ_{NL}) respectively. In addition to this, we have additional dependences on f_{NL} and g_{NL} implicit in the bias factors, as described in Section IV. This complex shape and scale dependence of the bispectrum offers an unique opportunity to simultaneously constrain f_{NL} , g_{NL} and τ_{NL} and thus distinguish between inflationary models. We will investigate this in the near future.

VIII. CONCLUSIONS

We have studied the growth of structure from non-Gaussian initial conditions of the local type. In particular, we have shown that the spatial distribution of dark-matter halos is naturally described by a multivariate local bias scheme where the halo number density depends on the underlying values of the density field δ , the auxiliary Gaussian potential φ , and (possibly) also on its gradient. This bivariate local approach can be equally interpreted as a non-local description in terms of δ only, since φ and δ are related by the Poisson equation. Adopting the peak-background split,

some common parameterizations of the halo mass function, and a local model for the evolution of large-scale density perturbations, we have derived the coefficients of this multivariate expansion as a function of the halo mass and of the parameters quantifying the level of primordial non-Gaussianity.

Using SPT to approximate the non-linear growth of density perturbations, we have computed the halo power spectrum and the halo-matter cross spectrum up to the third non-vanishing perturbative order. For unbiased tracers our result coincides with the matter power spectrum presented by [43]. However, in the most general (biased) case, it differs from what is obtained adopting the standard local bias expansion in terms of the density field [43–46]. The most remarkable feature is that the scale-dependent bias first discussed in Dal07 appears at leading order in our model for the power spectrum. This is because in our multivariate biasing scheme halo fluctuations on large scales trace the Gaussian potential φ rather than δ . However, our model reduces to the usual univariate case on larger scales, where the variance of density fluctuations is much larger than that of the potential. Note that both the multivariate and the univariate models predict that the dominant contribution to the halo power spectrum scales as $f_{\text{NL}} P_0(k)/\alpha(k)$ for $k \rightarrow 0$. However, for the standard univariate biasing, the amplitude of this term is given by a badly behaved integral which strongly depends on the assumed smoothing scale. Renormalization of the second bias coefficient (which should then be treated as a fitting parameter when comparing the theory to observation or simulations) is unavoidable in this case, while it is not needed in our model.

We have then tested our results against the N-body simulations by PPH08, finding excellent agreement for both the matter and the halo two-point functions. Focusing on the scale-dependent bias generated by primordial non-Gaussianity, we have shown that our model accounts for the discrepancies previously found between the predictions by Dal07 and the outcome of numerical simulations [40–42]. Corrections to the simpler model by Dal07 arise for two main reasons: (a) the bias coefficient b_{10} depends on f_{NL} due to the fact that the shape of the mass function is altered by primordial non-Gaussianity (see also [36, 39, 40]), and this adds a scale-independent offset to the bias deviation Δb ; (b) considering perturbation theory up to third order generates numerous additional corrective factors that become important on intermediate and small scales. With our one-loop calculation of the power spectrum, the range of validity of the theory extends up to scales $k \sim 0.1 - 0.3 h \text{ Mpc}^{-1}$ depending on halo mass and redshift.

We have also shown how our calculations can be extended to include higher-order terms of primordial non-Gaussianity, for instance by considering a non-vanishing primordial trispectrum proportional to the parameter g_{NL} . In this case, the halo power spectrum includes an additional contribution proportional to $g_{\text{NL}}^2 P_0(k)/\alpha^2(k)$ which, depending on the values of f_{NL} and g_{NL} , may be dominant on the largest scales. This term only appears in our multivariate expansion and originates from the bias parameter b_{02} which includes a correction proportional to g_{NL} . On the other hand, in agreement with [39], we have found that both the halo-halo and halo-matter spectra acquire a dependence on g_{NL} from the trispectrum of the linear density field. This term scales as $g_{\text{NL}} P_0(k)/\alpha(k)$ but its normalization depends on the assumed smoothing scale and cannot be robustly predicted by the theory.

Finally, we have calculated the halo bispectrum deriving from our multivariate biasing scheme. At tree level, our result corresponds to the usual bispectrum deriving from Gaussian initial conditions but where the linear bias b_{10} is replaced by $b_{10} + b_{01}/\alpha(k)$. This is different from what has been found assuming univariate local biasing [45, 46]. Therefore the analysis of three-point statistics represents a promising tool to test the different biasing schemes against observations. Also, the complex shape and scale dependence of the halo bispectrum offers an unique opportunity to simultaneously constrain f_{NL} , g_{NL} and τ_{NL} and thus put entire classes of inflationary models under scrutiny. We will explore this in more detail in a forthcoming paper.

Acknowledgments

We thank Christian T. Byrnes and Kazuya Koyama for useful discussions and comments on the draft, and Annalisa Pillepich for help with the simulation data. TG acknowledges support from the Alexander von Humboldt Foundation.

-
- [1] E. Komatsu et al. (WMAP) (2008), 0803.0547.
 - [2] J. M. Bardeen, J. R. Bond, N. Kaiser, and A. S. Szalay, *Astrophys. J.* **304**, 15 (1986).
 - [3] D. H. Lyth and A. Riotto, *Phys. Rept.* **314**, 1 (1999), hep-ph/9807278.
 - [4] J. M. Maldacena, *JHEP* **05**, 013 (2003), astro-ph/0210603.
 - [5] V. Acquaviva, N. Bartolo, S. Matarrese, and A. Riotto, *Nucl. Phys.* **B667**, 119 (2003), astro-ph/0209156.
 - [6] D. H. Lyth and D. Wands, *Phys. Lett.* **B524**, 5 (2002), hep-ph/0110002.
 - [7] A. D. Linde and V. F. Mukhanov, *Phys. Rev.* **D56**, 535 (1997), astro-ph/9610219.
 - [8] D. H. Lyth, C. Ungarelli, and D. Wands, *Phys. Rev.* **D67**, 023503 (2003), astro-ph/0208055.
 - [9] M. Sasaki, J. Valiviita, and D. Wands, *Phys. Rev.* **D74**, 103003 (2006), astro-ph/0607627.

- [10] K. A. Malik and D. H. Lyth, JCAP **0609**, 008 (2006), astro-ph/0604387.
- [11] F. Vernizzi and D. Wands, JCAP **0605**, 019 (2006), astro-ph/0603799.
- [12] J. Khoury, B. A. Ovrut, P. J. Steinhardt, and N. Turok, Phys. Rev. **D64**, 123522 (2001), hep-th/0103239.
- [13] P. Creminelli and L. Senatore, JCAP **0711**, 010 (2007), hep-th/0702165.
- [14] D. Polarski and A. A. Starobinsky, Phys. Rev. **D50**, 6123 (1994), astro-ph/9404061.
- [15] N. Bartolo, E. Komatsu, S. Matarrese, and A. Riotto, Phys. Rept. **402**, 103 (2004), astro-ph/0406398.
- [16] E. Komatsu et al. (2009), 0902.4759.
- [17] M. Tegmark et al. (SDSS), Phys. Rev. **D74**, 123507 (2006), astro-ph/0608632.
- [18] J. Valiviita and T. Giannantonio (2009), 0909.5190.
- [19] J. R. Fergusson and E. P. S. Shellard, Phys. Rev. **D80**, 043510 (2009), 0812.3413.
- [20] N. Bartolo, S. Matarrese, and A. Riotto, JHEP **04**, 006 (2004), astro-ph/0308088.
- [21] K. Enqvist and T. Takahashi, JCAP **0809**, 012 (2008), 0807.3069.
- [22] H. Assadullahi, J. Valiviita, and D. Wands, Phys. Rev. **D76**, 103003 (2007), 0708.0223.
- [23] Q.-G. Huang, JCAP **0811**, 005 (2008), 0808.1793.
- [24] C. T. Byrnes and G. Tasinato, JCAP **0908**, 016 (2009), 0906.0767.
- [25] Q.-G. Huang, JCAP **0906**, 035 (2009), 0904.2649.
- [26] K. M. Smith, L. Senatore, and M. Zaldarriaga, JCAP **0909**, 006 (2009), 0901.2572.
- [27] A. Curto, E. Martinez-Gonzalez, and R. B. Barreiro (2009), 0902.1523.
- [28] A. P. S. Yadav and B. D. Wandelt, Phys. Rev. Lett. **100**, 181301 (2008), 0712.1148.
- [29] P. Vielva and J. L. Sanz (2009), 0910.3196.
- [30] E. Komatsu and D. N. Spergel, Phys. Rev. **D63**, 063002 (2001), astro-ph/0005036.
- [31] R. Scoccimarro, E. Sefusatti, and M. Zaldarriaga, Phys. Rev. **D69**, 103513 (2004), astro-ph/0312286.
- [32] S. Matarrese, L. Verde, and R. Jimenez, Astrophys. J. **541**, 10 (2000), astro-ph/0001366.
- [33] M. LoVerde, A. Miller, S. Shandera, and L. Verde, JCAP **0804**, 014 (2008), 0711.4126.
- [34] N. Dalal, O. Dore, D. Huterer, and A. Shirokov, Phys. Rev. **D77**, 123514 (2008), 0710.4560.
- [35] S. Matarrese and L. Verde, Astrophys. J. **677**, L77 (2008), 0801.4826.
- [36] A. Slosar, C. Hirata, U. Seljak, S. Ho, and N. Padmanabhan, JCAP **0808**, 031 (2008), 0805.3580.
- [37] N. Afshordi and A. J. Tolley (2008), 0806.1046.
- [38] P. Valageas (2009), 0906.1042.
- [39] V. Desjacques and U. Seljak (2009), 0907.2257.
- [40] V. Desjacques, U. Seljak, and I. Iliev (2008), 0811.2748.
- [41] A. Pillepich, C. Porciani, and O. Hahn (2008), 0811.4176.
- [42] M. Grossi, L. Verde, C. Carbone, K. Dolag, E. Branchini, F. Iannuzzi, S. Matarrese, and L. Moscardini, Mon. Not. R. Astron. Soc. **398**, 321 (2009), 0902.2013.
- [43] A. Taruya, K. Koyama, and T. Matsubara, Phys. Rev. **D78**, 123534 (2008), 0808.4085.
- [44] E. Sefusatti (2009), 0905.0717.
- [45] E. Sefusatti and E. Komatsu, Phys. Rev. **D76**, 083004 (2007), 0705.0343.
- [46] D. Jeong and E. Komatsu, Astrophys. J. **703**, 1230 (2009), 0904.0497.
- [47] P. McDonald, Phys. Rev. **D78**, 123519 (2008), 0806.1061.
- [48] J. N. Fry and E. Gaztanaga, Astrophys. J. **413**, 447 (1993), astro-ph/9302009.
- [49] R. S. Somerville, G. Lemson, Y. Sigad, A. Dekel, G. Kauffmann, and S. D. M. White, Mon. Not. R. Astron. Soc. **320**, 289 (2001), arXiv:astro-ph/9912073.
- [50] S. Cole and N. Kaiser, Mon. Not. Roy. Astron. Soc. **237**, 1127 (1989).
- [51] H. J. Mo and S. D. M. White, Mon. Not. Roy. Astron. Soc. **282**, 347 (1996), astro-ph/9512127.
- [52] P. Catelan, F. Lucchin, S. Matarrese, and C. Porciani, Mon. Not. Roy. Astron. Soc. **297**, 692 (1998), astro-ph/9708067.
- [53] R. K. Sheth and G. Tormen, Mon. Not. Roy. Astron. Soc. **308**, 119 (1999), astro-ph/9901122.
- [54] P. Catelan, C. Porciani, and M. Kamionkowski, Mon. Not. Roy. Astron. Soc. **318**, 39 (2000), astro-ph/0005544.
- [55] H. J. Mo, Y. P. Jing, and S. D. M. White, Mon. Not. Roy. Astron. Soc. **282**, 1096 (1996), astro-ph/9602052.
- [56] T. Matsubara, Phys. Rev. **D78**, 083519 (2008), 0807.1733.
- [57] A. F. Heavens, S. Matarrese, and L. Verde, Mon. Not. Roy. Astron. Soc. **301**, 797 (1998), astro-ph/9808016.
- [58] W. H. Press and P. Schechter, Astrophys. J. **187**, 425 (1974).
- [59] A. Jenkins et al., Mon. Not. Roy. Astron. Soc. **321**, 372 (2001), astro-ph/0005260.
- [60] M. S. Warren, K. Abazajian, D. E. Holz, and L. Teodoro, Astrophys. J. **646**, 881 (2006), astro-ph/0506395.
- [61] J. L. Tinker et al. (2008), 0803.2706.
- [62] R. K. Sheth and G. Tormen, Mon. Not. Roy. Astron. Soc. **329**, 61 (2002), astro-ph/0105113.
- [63] M. Maggiore and A. Riotto (2009), 0903.1251.
- [64] T. Y. Lam and R. K. Sheth, ArXiv e-prints (2009), 0905.1702.
- [65] F. Bernardeau, Astron. Astrophys. **291**, 697 (1994), astro-ph/9403020.
- [66] P. McDonald, Phys. Rev. **D74**, 103512 (2006), astro-ph/0609413.
- [67] R. E. Smith, R. Scoccimarro, and R. K. Sheth, Phys. Rev. **D75**, 063512 (2007), astro-ph/0609547.
- [68] J. Carlson, M. White, and N. Padmanabhan (2009), 0905.0479.
- [69] M. Crocce and R. Scoccimarro, Phys. Rev. **D73**, 063519 (2006), astro-ph/0509418.
- [70] M. Crocce and R. Scoccimarro, Phys. Rev. **D73**, 063520 (2006), astro-ph/0509419.
- [71] A. Taruya and T. Hiramatsu (2007), 0708.1367.

[72] M. Pietroni, JCAP **0810**, 036 (2008), 0806.0971.

[73] P. McDonald, Phys. Rev. **D75**, 043514 (2007), astro-ph/0606028.

[74] T. Matsubara, Phys. Rev. **D77**, 063530 (2008), 0711.2521.

[75] J. R. Bond and A. H. Jaffe, Royal Society of London Philosophical Transactions Series A **357**, 57 (1999), arXiv:astro-ph/9809043.

Appendix: Complete analytic expression of the power spectra

We list below the non-vanishing contributions to the halo-halo and halo-matter power spectra up to one-loop in perturbation theory. These have been obtained by smoothing the evolved density perturbations with the filter $W(kR)$, so that $\tilde{\delta}(k) \rightarrow \tilde{\delta}(k, R) = \tilde{\delta}(k) W(kR)$. We highlight with the label ‘‘Local’’ the terms that are also present if we use the univariate local bias approach as in [43]. Similarly, the contributions that do not vanish in the Gaussian case are marked with the label ‘‘Gauss’’. We have dropped the two-loop terms which arise from the trispectrum T_0 , as they generally give negligible contributions, with the exception of the term $P_{13}^{II}(k, R)$, which is important in the case of large g_{NL} and small f_{NL} . Some of the integrals below present an infrared divergence if $n_s \simeq 1$, like for instance the term $P_{(23)(23)}^{hh}$. In this case, we introduce a cutoff in $P_0(k)$ for $k < k_H = 1/R_H$ where $R_H = c/H_0$ [75].

Note that only the halo-matter cross spectrum has been compared to the N-body results by PPH08, as in the simulations the halo-halo spectrum is more strongly affected by shot noise.

1. The halo-halo spectrum

The full halo-halo power spectrum at one loop is

$$P^{hh}(k, z, R) = D^2(z) P_{11}^{hh}(k, R) + D^3(z) P_{12}^{hh}(k, R) + D^4(z) [P_{22}^{hh}(k, R) + P_{13}^{hh}(k, R)], \quad (77)$$

where:

$P_{11}^{hh}(k, R)$ is the sum of the following terms:

$$\begin{aligned} \text{Local, Gauss } P_{(10)(10)}^{hh}(k, R) &= b_{10}^2 P_0(k) W^2(kR) \\ 2P_{(10)(11)}^{hh}(k, R) &= 2 b_{10} b_{01} \frac{P_0(k)}{\alpha(k)} W^2(kR) \\ P_{(11)(11)}^{hh}(k, R) &= b_{01}^2 \frac{P_0(k)}{\alpha^2(k)} W^2(kR). \end{aligned} \quad (78)$$

$P_{12}^{hh}(k, R)$ is the sum of the following terms:

$$\begin{aligned} \text{Local } 2P_{(10)(20)}^{hh}(k, R) &= 2 b_{10}^2 \int \frac{d^3 \mathbf{q}}{(2\pi)^3} B_0(\mathbf{k}, \mathbf{q}, -\mathbf{k} - \mathbf{q}) J_2^{(s)}(-\mathbf{k} - \mathbf{q}, \mathbf{q}) W^2(kR) W^2(qR) \\ 2P_{(11)(20)}^{hh}(k, R) &= 2 b_{01} b_{10} \int \frac{d^3 \mathbf{q}}{(2\pi)^3} \frac{B_0(\mathbf{k}, \mathbf{q}, -\mathbf{k} - \mathbf{q})}{\alpha(k)} J_2^{(s)}(-\mathbf{k} - \mathbf{q}, \mathbf{q}) W^2(kR) W^2(qR) \\ \text{Local } 2P_{(10)(21)}^{hh}(k, R) &= b_{10} b_{20} \int \frac{d^3 \mathbf{q}}{(2\pi)^3} B_0(\mathbf{k}, \mathbf{q}, -\mathbf{k} - \mathbf{q}) W(kR) W(qR) W(|\mathbf{k} + \mathbf{q}|R) \\ 2P_{(11)(21)}^{hh}(k, R) &= b_{01} b_{20} \int \frac{d^3 \mathbf{q}}{(2\pi)^3} \frac{B_0(\mathbf{k}, \mathbf{q}, -\mathbf{k} - \mathbf{q})}{\alpha(k)} W(kR) W(qR) W(|\mathbf{k} + \mathbf{q}|R) \\ 2P_{(10)(22)}^{hh}(k, R) &= b_{10} b_{11} \int \frac{d^3 \mathbf{q}}{(2\pi)^3} \frac{B_0(\mathbf{k}, \mathbf{q}, -\mathbf{k} - \mathbf{q})}{\alpha(q)} W(kR) W(qR) W(|\mathbf{k} + \mathbf{q}|R) \\ 2P_{(11)(22)}^{hh}(k, R) &= b_{01} b_{11} \int \frac{d^3 \mathbf{q}}{(2\pi)^3} \frac{B_0(\mathbf{k}, \mathbf{q}, -\mathbf{k} - \mathbf{q})}{\alpha(k) \alpha(q)} W(kR) W(qR) W(|\mathbf{k} + \mathbf{q}|R) \\ 2P_{(10)(23)}^{hh}(k, R) &= b_{10} b_{02} \int \frac{d^3 \mathbf{q}}{(2\pi)^3} \frac{B_0(\mathbf{k}, \mathbf{q}, -\mathbf{k} - \mathbf{q})}{\alpha(q) \alpha(|\mathbf{k} + \mathbf{q}|)} W(kR) W(qR) W(|\mathbf{k} + \mathbf{q}|R) \\ 2P_{(11)(23)}^{hh}(k, R) &= b_{01} b_{02} \int \frac{d^3 \mathbf{q}}{(2\pi)^3} \frac{B_0(\mathbf{k}, \mathbf{q}, -\mathbf{k} - \mathbf{q})}{\alpha(k) \alpha(q) \alpha(|\mathbf{k} + \mathbf{q}|)} W(kR) W(qR) W(|\mathbf{k} + \mathbf{q}|R). \end{aligned} \quad (79)$$

$P_{22}^{hh}(k, R)$ is the sum of the following terms:

$$\begin{aligned}
\text{Local, Gauss } P_{(20)(20)}^{hh}(k, R) &= 2 b_{10}^2 \int \frac{d^3 \mathbf{q}}{(2\pi)^3} P_0(q) P_0(|\mathbf{k} - \mathbf{q}|) \left[J_2^{(s)}(\mathbf{q}, \mathbf{k} - \mathbf{q}) \right]^2 W^2(kR) \\
\text{Local, Gauss } 2P_{(20)(21)}^{hh}(k, R) &= 2 b_{10} b_{20} \int \frac{d^3 \mathbf{q}}{(2\pi)^3} P_0(q) P_0(|\mathbf{k} - \mathbf{q}|) J_2^{(s)}(\mathbf{q}, \mathbf{k} - \mathbf{q}) W(kR) W(qR) W(|\mathbf{k} - \mathbf{q}|R) \\
\text{Local, Gauss } P_{(21)(21)}^{hh}(k, R) &= \frac{1}{2} b_{20}^2 \int \frac{d^3 \mathbf{q}}{(2\pi)^3} P_0(q) P_0(|\mathbf{k} - \mathbf{q}|) W^2(qR) W^2(|\mathbf{k} - \mathbf{q}|R) \\
2P_{(20)(22)}^{hh}(k, R) &= 2 b_{10} b_{11} \int \frac{d^3 \mathbf{q}}{(2\pi)^3} \frac{P_0(q)}{\alpha(q)} P_0(|\mathbf{k} - \mathbf{q}|) J_2^{(s)}(\mathbf{q}, \mathbf{k} - \mathbf{q}) W(kR) W(qR) W(|\mathbf{k} - \mathbf{q}|R) \\
2P_{(21)(22)}^{hh}(k, R) &= b_{20} b_{11} \int \frac{d^3 \mathbf{q}}{(2\pi)^3} \frac{P_0(q)}{\alpha(q)} P_0(|\mathbf{k} - \mathbf{q}|) W^2(qR) W^2(|\mathbf{k} - \mathbf{q}|R) \\
P_{(22)(22)}^{hh}(k, R) &= \frac{1}{4} b_{11}^2 \int \frac{d^3 \mathbf{q}}{(2\pi)^3} \left[P_0(q) \frac{P_0(|\mathbf{k} - \mathbf{q}|)}{\alpha(|\mathbf{k} - \mathbf{q}|)^2} + \frac{P_0(q)}{\alpha(q)} \frac{P_0(|\mathbf{k} - \mathbf{q}|)}{\alpha(|\mathbf{k} - \mathbf{q}|)} \right] W^2(qR) W^2(|\mathbf{k} - \mathbf{q}|R) \\
2P_{(20)(23)}^{hh}(k, R) &= 2 b_{10} b_{02} \int \frac{d^3 \mathbf{q}}{(2\pi)^3} \frac{P_0(q)}{\alpha(q)} \frac{P_0(|\mathbf{k} - \mathbf{q}|)}{\alpha(|\mathbf{k} - \mathbf{q}|)} J_2^{(s)}(\mathbf{q}, \mathbf{k} - \mathbf{q}) W(kR) W(qR) W(|\mathbf{k} - \mathbf{q}|R) \\
2P_{(21)(23)}^{hh}(k, R) &= b_{20} b_{02} \int \frac{d^3 \mathbf{q}}{(2\pi)^3} \frac{P_0(q)}{\alpha(q)} \frac{P_0(|\mathbf{k} - \mathbf{q}|)}{\alpha(|\mathbf{k} - \mathbf{q}|)} W^2(qR) W^2(|\mathbf{k} - \mathbf{q}|R) \\
2P_{(22)(23)}^{hh}(k, R) &= b_{11} b_{02} \int \frac{d^3 \mathbf{q}}{(2\pi)^3} \frac{P_0(q)}{\alpha(q)} \frac{P_0(|\mathbf{k} - \mathbf{q}|)}{\alpha^2(|\mathbf{k} - \mathbf{q}|)} W^2(qR) W^2(|\mathbf{k} - \mathbf{q}|R) \\
P_{(23)(23)}^{hh}(k, R) &= \frac{1}{2} b_{02}^2 \int \frac{d^3 \mathbf{q}}{(2\pi)^3} \frac{P_0(q)}{\alpha^2(q)} \frac{P_0(|\mathbf{k} - \mathbf{q}|)}{\alpha^2(|\mathbf{k} - \mathbf{q}|)} W^2(qR) W^2(|\mathbf{k} - \mathbf{q}|R). \tag{80}
\end{aligned}$$

$P_{13}^{hh}(k, R)$ is the sum of the following terms:

$$\begin{aligned}
\text{Local, Gauss } 2P_{(10)(30)}^{hh}(k, R) &= 6 b_{10}^2 P_0(k) \int \frac{d^3 \mathbf{q}}{(2\pi)^3} P_0(q) J_3^{(s)}(\mathbf{k}, \mathbf{q}, -\mathbf{q}) W^2(kR) \\
2P_{(11)(30)}^{hh}(k, R) &= 6 b_{01} b_{10} \frac{P_0(k)}{\alpha(k)} \int \frac{d^3 \mathbf{q}}{(2\pi)^3} P_0(q) J_3^{(s)}(\mathbf{k}, \mathbf{q}, -\mathbf{q}) W^2(kR) \\
\text{Local, Gauss } 2P_{(10)(31)}^{hh}(k, R) &= 4 b_{10} b_{20} P_0(k) \int \frac{d^3 \mathbf{q}}{(2\pi)^3} P_0(q) J_2^{(s)}(\mathbf{q}, \mathbf{k}) W(kR) W(qR) W(|\mathbf{k} + \mathbf{q}|R) \\
2P_{(11)(31)}^{hh}(k, R) &= 4 b_{01} b_{20} \frac{P_0(k)}{\alpha(k)} \int \frac{d^3 \mathbf{q}}{(2\pi)^3} P_0(q) J_2^{(s)}(\mathbf{q}, \mathbf{k}) W(kR) W(qR) W(|\mathbf{k} + \mathbf{q}|R) \\
2P_{(10)(32)}^{hh}(k, R) &= 2 b_{10} b_{11} P_0(k) \int \frac{d^3 \mathbf{q}}{(2\pi)^3} \frac{P_0(q)}{\alpha(q)} J_2^{(s)}(\mathbf{q}, \mathbf{k}) W(kR) W(qR) W(|\mathbf{k} + \mathbf{q}|R) \\
2P_{(11)(32)}^{hh}(k, R) &= 2 b_{01} b_{11} \frac{P_0(k)}{\alpha(k)} \int \frac{d^3 \mathbf{q}}{(2\pi)^3} \frac{P_0(q)}{\alpha(q)} J_2^{(s)}(\mathbf{q}, \mathbf{k}) W(kR) W(qR) W(|\mathbf{k} + \mathbf{q}|R) \\
2P_{(10)(33)}^{hh}(k, R) &= \frac{2}{3} b_{10} b_{21} P_0(k) \int \frac{d^3 \mathbf{q}}{(2\pi)^3} \frac{P_0(q)}{\alpha(q)} W^2(kR) W^2(qR) \\
2P_{(11)(33)}^{hh}(k, R) &= \frac{2}{3} b_{01} b_{21} \frac{P_0(k)}{\alpha(k)} \int \frac{d^3 \mathbf{q}}{(2\pi)^3} \frac{P_0(q)}{\alpha(q)} W^2(kR) W^2(qR) \\
2P_{(10)(34)}^{hh}(k, R) &= \frac{1}{3} b_{10} b_{12} P_0(k) \int \frac{d^3 \mathbf{q}}{(2\pi)^3} P_0(q) \left[\frac{1}{\alpha^2(q)} + \frac{1}{\alpha(k) \alpha(q)} \right] W^2(kR) W^2(qR) \\
2P_{(11)(34)}^{hh}(k, R) &= \frac{1}{3} b_{01} b_{12} \frac{P_0(k)}{\alpha(k)} \int \frac{d^3 \mathbf{q}}{(2\pi)^3} P_0(q) \left[\frac{1}{\alpha^2(q)} + \frac{1}{\alpha(k) \alpha(q)} \right] W^2(kR) W^2(qR)
\end{aligned}$$

$$\begin{aligned}
\text{Local, Gauss } 2P_{(10)(35)}^{hh}(k, R) &= b_{10} b_{30} P_0(k) \int \frac{d^3 \mathbf{q}}{(2\pi)^3} P_0(q) W^2(kR) W^2(qR) \\
2P_{(11)(35)}^{hh}(k, R) &= b_{01} b_{30} \frac{P_0(k)}{\alpha(k)} \int \frac{d^3 \mathbf{q}}{(2\pi)^3} P_0(q) W^2(kR) W^2(qR) \\
2P_{(10)(36)}^{hh}(k, R) &= b_{10} b_{03} \frac{P_0(k)}{\alpha(k)} \int \frac{d^3 \mathbf{q}}{(2\pi)^3} \frac{P_0(q)}{\alpha^2(q)} W^2(kR) W^2(qR) \\
2P_{(11)(36)}^{hh}(k, R) &= b_{01} b_{03} \frac{P_0(k)}{\alpha^2(k)} \int \frac{d^3 \mathbf{q}}{(2\pi)^3} \frac{P_0(q)}{\alpha^2(q)} W^2(kR) W^2(qR). \tag{81}
\end{aligned}$$

The only important two-loop contribution is (relevant for small f_{NL} , large g_{NL}):

$$P_{13}^{hh, II}(k, R) = \frac{1}{3} b_{10} b_{30} \int \frac{d^3 \mathbf{q} d^3 \mathbf{p}}{(2\pi)^6} T_0(\mathbf{k}, \mathbf{q}, \mathbf{p}, -\mathbf{k} - \mathbf{q} - \mathbf{p}) W(qR) W(pR) W(|\mathbf{q} + \mathbf{p}|R) W(|-\mathbf{k} - \mathbf{q} - \mathbf{p}|R). \tag{82}$$

2. The halo-matter spectrum

The full halo-matter cross spectrum at one loop is

$$P^{hm}(k, z, R) = D^2(z) P_{11}^{hm}(k, R) + D^3(z) P_{12}^{hm}(k, R) + D^4(z) [P_{22}^{hm}(k, R) + P_{13}^{hm}(k, R)]. \tag{83}$$

$P_{11}^{hm}(k, R)$ is the sum of the following terms:

$$\begin{aligned}
\text{Local, Gauss } P_{(10)(10)}^{hm}(k, R) &= b_{10} P_0(k) W^2(kR) \\
P_{(10)(11)}^{hm}(k, R) &= b_{01} \frac{P_0(k)}{\alpha(k)} W^2(kR). \tag{84}
\end{aligned}$$

$P_{12}^{hm}(k, R)$ is the sum of the following terms:

$$\begin{aligned}
\text{Local } 2P_{(10)(20)}^{hm}(k, R) &= 2b_{10} \int \frac{d^3 \mathbf{q}}{(2\pi)^3} B_0(\mathbf{k}, \mathbf{q}, -\mathbf{k} - \mathbf{q}) J_2^{(s)}(-\mathbf{k} - \mathbf{q}, \mathbf{q}) W^2(kR) W^2(qR) \\
P_{(11)(20)}^{hm}(k, R) &= b_{01} \int \frac{d^3 \mathbf{q}}{(2\pi)^3} \frac{B_0(\mathbf{k}, \mathbf{q}, -\mathbf{k} - \mathbf{q})}{\alpha(k)} J_2^{(s)}(-\mathbf{k} - \mathbf{q}, \mathbf{q}) W^2(kR) W^2(qR) \\
\text{Local } P_{(10)(21)}^{hm}(k, R) &= \frac{1}{2} b_{20} \int \frac{d^3 \mathbf{q}}{(2\pi)^3} B_0(\mathbf{k}, \mathbf{q}, -\mathbf{k} - \mathbf{q}) W(kR) W(qR) W(|\mathbf{k} + \mathbf{q}|R) \\
P_{(10)(22)}^{hm}(k, R) &= \frac{1}{2} b_{11} \int \frac{d^3 \mathbf{q}}{(2\pi)^3} \frac{B_0(\mathbf{k}, \mathbf{q}, -\mathbf{k} - \mathbf{q})}{\alpha(q)} W(kR) W(qR) W(|\mathbf{k} + \mathbf{q}|R) \\
P_{(10)(23)}^{hm}(k, R) &= \frac{1}{2} b_{02} \int \frac{d^3 \mathbf{q}}{(2\pi)^3} \frac{B_0(\mathbf{k}, \mathbf{q}, -\mathbf{k} - \mathbf{q})}{\alpha(q) \alpha(|\mathbf{k} + \mathbf{q}|)} W(kR) W(qR) W(|\mathbf{k} + \mathbf{q}|R). \tag{85}
\end{aligned}$$

$P_{22}^{hm}(k, R)$ is the sum of the following terms:

$$\begin{aligned}
\text{Local, Gauss } P_{(20)(20)}^{hm}(k, R) &= 2b_{10} \int \frac{d^3 \mathbf{q}}{(2\pi)^3} P_0(q) P_0(|\mathbf{k} - \mathbf{q}|) \left[J_2^{(s)}(\mathbf{q}, \mathbf{k} - \mathbf{q}) \right]^2 W^2(kR) \\
\text{Local, Gauss } P_{(20)(21)}^{hm}(k, R) &= b_{20} \int \frac{d^3 \mathbf{q}}{(2\pi)^3} P_0(q) P_0(|\mathbf{k} - \mathbf{q}|) J_2^{(s)}(\mathbf{q}, \mathbf{k} - \mathbf{q}) W(kR) W(qR) W(|\mathbf{k} - \mathbf{q}|R) \\
P_{(20)(22)}^{hm}(k, R) &= b_{11} \int \frac{d^3 \mathbf{q}}{(2\pi)^3} \frac{P_0(q)}{\alpha(q)} P_0(|\mathbf{k} - \mathbf{q}|) J_2^{(s)}(\mathbf{q}, \mathbf{k} - \mathbf{q}) W(kR) W(qR) W(|\mathbf{k} - \mathbf{q}|R) \\
P_{(20)(23)}^{hm}(k, R) &= b_{02} \int \frac{d^3 \mathbf{q}}{(2\pi)^3} \frac{P_0(q)}{\alpha(q)} \frac{P_0(|\mathbf{k} - \mathbf{q}|)}{\alpha(|\mathbf{k} - \mathbf{q}|)} J_2^{(s)}(\mathbf{q}, \mathbf{k} - \mathbf{q}) W(kR) W(qR) W(|\mathbf{k} - \mathbf{q}|R). \tag{86}
\end{aligned}$$

$P_{13}^{hm}(k, R)$ is the sum of the following terms:

$$\begin{aligned}
\text{Local, Gauss } 2P_{(10)(30)}^{hm}(k, R) &= 6 b_{10} P_0(k) \int \frac{d^3 \mathbf{q}}{(2\pi)^3} P_0(q) J_3^{(s)}(\mathbf{k}, \mathbf{q}, -\mathbf{q}) W^2(kR) \\
P_{(11)(30)}^{hm}(k, R) &= 3 b_{01} \frac{P_0(k)}{\alpha(k)} \int \frac{d^3 \mathbf{q}}{(2\pi)^3} P_0(q) J_3^{(s)}(\mathbf{k}, \mathbf{q}, -\mathbf{q}) W^2(kR) \\
\text{Local, Gauss } P_{(10)(31)}^{hm}(k, R) &= 2 b_{20} P(k) \int \frac{d^3 \mathbf{q}}{(2\pi)^3} P_0(q) J_2^{(s)}(\mathbf{q}, \mathbf{k}) W(kR) W(qR) W(|\mathbf{k} + \mathbf{q}|R) \\
P_{(10)(32)}^{hm}(k, R) &= b_{11} P_0(k) \int \frac{d^3 \mathbf{q}}{(2\pi)^3} \frac{P_0(q)}{\alpha(q)} J_2^{(s)}(\mathbf{q}, \mathbf{k}) W(kR) W(qR) W(|\mathbf{k} + \mathbf{q}|R) \\
P_{(10)(33)}^{hm}(k, R) &= \frac{1}{3} b_{21} P_0(k) \int \frac{d^3 \mathbf{q}}{(2\pi)^3} \frac{P_0(q)}{\alpha(q)} W^2(kR) W^2(qR) \\
P_{(10)(34)}^{hm}(k, R) &= \frac{1}{6} b_{12} P_0(k) \int \frac{d^3 \mathbf{q}}{(2\pi)^3} P_0(q) \left[\frac{1}{\alpha^2(q)} + \frac{1}{\alpha(k)\alpha(q)} \right] W^2(kR) W^2(qR) \\
\text{Local, Gauss } P_{(10)(35)}^{hm}(k, R) &= \frac{1}{3} b_{30} P_0(k) \int \frac{d^3 \mathbf{q}}{(2\pi)^3} P_0(q) W^2(kR) W^2(qR) \\
P_{(10)(36)}^{hm}(k, R) &= \frac{1}{3} b_{03} \frac{P_0(k)}{\alpha(k)} \int \frac{d^3 \mathbf{q}}{(2\pi)^3} \frac{P_0(q)}{\alpha^2(q)} W^2(kR) W^2(qR). \tag{87}
\end{aligned}$$

The only important two-loop contribution is (relevant for small f_{NL} , large g_{NL}):

$$P_{13}^{hm, II}(k, R) = \frac{1}{6} b_{30} \int \frac{d^3 \mathbf{q} d^3 \mathbf{p}}{(2\pi)^6} T_0(\mathbf{k}, \mathbf{q}, \mathbf{p}, -\mathbf{k} - \mathbf{q} - \mathbf{p}) W(qR) W(pR) W(|\mathbf{q} + \mathbf{p}|R) W(|-\mathbf{k} - \mathbf{q} - \mathbf{p}|R). \tag{88}$$